TU Delft

Delft University of Technology

Influence of indirectly heated steam-blown gasification process conditions on biochar physico-chemical properties

Del Grosso, Mara; Cutz, Luis; Tiringer, Urša; Tsekos, Christos; Taheri, Peyman; de Jong, Wiebren

DOI
10.1016/j.fuproc.2022.107347

Publication date
2022

Document Version
Final published version

Published in
Fuel Processing Technology

Citation (APA)
Del Grosso, M., Cutz, L., Tiringer, U., Tsekos, C., Taheri, P., & de Jong, W. (2022). Influence of indirectly heated steam-blown gasification process conditions on biochar physico-chemical properties. *Fuel Processing Technology*, *235*, Article 107347. https://doi.org/10.1016/j.fuproc.2022.107347

Important note
To cite this publication, please use the final published version (if applicable).
Please check the document version above.

Copyright
Other than for strictly personal use, it is not permitted to download, forward or distribute the text or part of it, without the consent of the author(s) and/or copyright holder(s), unless the work is under an open content license such as Creative Commons.

Takedown policy
Please contact us and provide details if you believe this document breaches copyrights.
We will remove access to the work immediately and investigate your claim.

This work is downloaded from Delft University of Technology.
For technical reasons the number of authors shown on this cover page is limited to a maximum of 10.

Fuel Processing Technology 235 (2022) 107347

Contents lists available at ScienceDirect

Fuel Processing Technology

journal homepage: www.elsevier.com/locate/fuproc

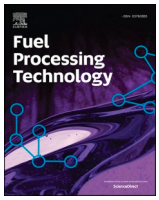

Influence of indirectly heated steam-blown gasification process conditions on biochar physico-chemical properties

Mara Del Grosso [a,*,1], Luis Cutz [a,*,1], Urša Tiringer [b], Christos Tsekos [a], Peyman Taheri [b], Wiebren de Jong [a]

[a] Process and Energy Department, University of Technology of Delft, Leeghwaterstraat 39, 2628 CB Delft, the Netherlands
[b] Material Science and Engineering Department, Mekelweg 2, 2628 CD Delft, the Netherlands

ARTICLE INFO

Keywords:
Biochar
Gasification
Surface Analysis
Characterization techniques

ABSTRACT

Our work provides a thorough characterization of different biochars produced by a novel 50 kW_{th} Indirectly Heated Bubbling Fluidized Bed Steam Reformer. This study investigates the effect of temperature and gasification agent on the physico-chemical properties of biochars. We combined macro, micro and nano characterization techniques to provide a clear picture of the biochar characteristics, surface functionality and its "inert" nature toward potential applications. Our results demonstrate that indirect gasification is capable of producing carbon-rich biochars (> 92%) with increased porosity (89–198 $cm^3.g^{-1}$), high heating value (28–31 $MJ.kg^{-1}$ a.r.) and aromaticity compared to the parent biomass. All biochars have lower O/C (0.02–0.04) and H/C atomic ratios (0.09–0.19), similar to anthracite. For the range of tested gasification conditions, air/steam gasification at an equivalence ratio of 0.20 and steam-to-biomass ratio of 1.2 provides the highest biochar yield (7.3%), while maintaining syngas composition optimal. On the other hand, air gasification produces biochars with relatively high content of inorganic elements. Indirectly heated biochars are compliant with the European Biochar Certificate regarding the carbon content, O/C ratio, H/C ratio. Our biochars may provide an improvement in agricultural yield and CO_2 adsorption, especially those produced under air/steam gasification conditions. Our novel indirect design not only constitutes a promising development in the field of biomass allothermal gasification but also can help improving gasification circularity through the production of high quality biochar.

1. Introduction

During the last 20 years, there has been an extensive focus on using biomass as a source of renewable energy [1]. Several feedstocks and technologies are used to convert biomass into energy-dense intermediates that later on can be transformed into solid, liquid and gaseous fuels [2]. Among the different pathways to convert biomass, thermochemical routes provide versatility in terms of feedstocks (e.g., forest, agricultural and municipal residues) and products (solid, liquid and gas) compared to other renewable technologies such as solar, wind, hydro and geothermal. In general, all thermochemical processes (e.g., pyrolysis, gasification and combustion) and corresponding regimes (e.g., hydrothermal carbonization, torrefaction and liquefaction) produce three types of co-products: solid material (biochar/bio-coal and ash), condensable (e.g., bio-oil) and non-condensable gases (syngas) [3–6]. Up to now, most attention has been placed on producing, characterizing and upgrading bio-oil and syngas for energy purposes [7,8]. Nevertheless, the valorisation of biochar still remains limited. This is because biochar is still seen as a secondary product. It is rarely the case that thermochemical processes are only oriented to biochar production, except for slow pyrolysis.

Herein, biochar is defined as the solid material obtained from the carbonization of biomass in an oxygen-limited environment during thermochemical conversion [9]. Recent research on biochar has drawn attention to novel properties which have opened the door to a list of more than fifty applications such as soil conditioner, solid fuel for direct/co-combustion, biogas production, wastewater treatment, and utilization in the building, textile and wellness sector [10–12]. Many of them are carbon sinks and provide a net reduction of greenhouse gas (GHG) emissions in the life-cycle of thermochemical processes [11,13]. Each end-use application requires biochars with specific properties which, in turn, are produced by the careful selection of the feedstock,

* Corresponding authors.
E-mail addresses: M.delGrosso@tudelft.nl (M. Del Grosso), luis.cutz@tudelft.nl (L. Cutz).
[1] These authors have equally contributed to this work.

https://doi.org/10.1016/j.fuproc.2022.107347
Received 22 December 2021; Received in revised form 1 June 2022; Accepted 1 June 2022
Available online 21 June 2022
0378-3820/© 2022 The Authors. Published by Elsevier B.V. This is an open access article under the CC BY license (http://creativecommons.org/licenses/by/4.0/).

thermochemical technology and process conditions (e.g., heating rate, operation temperature and residence time). Classification of different thermochemical processes in terms of operating conditions and biochar yields are summarized in **Supplementary Information – Section A**. Within the wide portfolio of thermochemical technologies there is no single "winner". Each technology has its own advantages and their selection will depend on the type of feedstock, scale and desired product.

In this paper we focused on biochar produced from gasification. Regardless of the biochar yield, further use of the biochar offers the opportunity to improve the circularity of gasification, while maximizing the use of biomass. A detailed search using Scopus database and keywords "gasification biochar" or "biochar from gasification" reports >15,000 scientific publications and/or reports since 2012. Nevertheless, few studies in literature produced biochar from gasification and proposed possible applications based on its properties. Most commonly studied gasifiers, feedstocks, operating temperature and gasifying agent in this respect are summarized in Table 1.

The studies reported in Table 1 show the key role played by the interaction among process production parameters on biochar properties and, therefore, on its possible post process applications. In general, according to literature, the increase of process temperature results to be a key factor for a more stable biochar (higher carbon content) with higher surface area, albeit with reduced yields. Less amount of biochar is also obtained with a more oxidative environment. The use of steam as gasification agent, on the other hand, is responsible for higher surface area and pore volume. Last but not least, the nature of the parent biomass highly influences the elemental composition and functionalities of the biochar produced.

Typical characterization techniques of biochars are the following: elemental and proximate analysis, nitrogen gas sorption analysis, Brunauer-Emmett-Teller (BET), biochar pH, scanning electron microscopy coupled with Energy Dispersive X-ray Spectroscopy (SEM-EDS), bomb calorimetry, Fourier Transform Infrared Spectroscopy (FTIR), quantitative ^{13}C nuclear magnetic resonance spectroscopy (NMR), X-ray fluorescence analysis (XRF) and X-Ray powder Diffraction (XRD) [12,16,18,20].

Instead of selecting an application for biochar and performing a thorough characterization, here we revert this framework and suggest potential applications depending on the biochar physico-chemical properties and surface characterization.

Our work aims to extend existing knowledge on gasification derived biochar by providing a thorough characterization of such biochars produced from woody biomass using a novel pilot scale 50 kW_{th} Indirectly Heated Bubbling Fluidized Bed Steam Reformer (IHBFBSR) [21]. It is the first time that biochar produced from this unique reactor is characterized. The novelty of the gasifier consists on its configuration: unlike similar indirectly heated designs [22–24], in the IHBFBSR unit, the combustion (in the radiant tube burners) and gasification (in the fluidized bed reformer) zones are completely separated and the heat is transferred from inside toward outside. Results of our previous work [21] demonstrated that, overall, the IHBFBSR technology might play an important role in the next generation of gasification reactors, considering the increased interest from industry toward high yields of undiluted syngas and hydrogen production. Product gas composition and cold gas efficiency (CGE)[2] obtained from the new design were found to be favorably compared to some similar allothermal gasification systems while carbon conversion could be improved.

Therefore, in the present work, we investigated four biochars produced at different temperatures, using different gasifying agents and particle size of the bed material. In the present work, only results related to biochar production are included. We suggest potential applications for the biochars depending on their physico-chemical properties. The obtained high quality biochars improve the circularity of the process and confirm our novel indirect design as promising development in the field of biomass allothermal gasification. Moreover, our findings will contribute to improve the process design of future scale-up of our reactor and similar designs based on radiant tubes.

The parent biomass and biochars were characterized by means of Proximate and Ultimate Analysis, High Heating Value (HHV), SEM-EDS, XRD, XRF, BET and X-ray Photoelectron Spectroscopy (XPS). The obtained results were integrated to suggest possible applications and highlight challenges regarding the use gasification biochar.

2. Materials and methods

2.1. Materials production and collection

The biomass used for all experiments is an A-quality secondary forest wood (termed Premium Green) obtained from woodchips, sawdust and wood shavings from brown leafage wood from the Netherlands. The biomass was obtained from the Dutch company Labee Group Moerdijk B·V. and it was provided as pellets with an approximate length of 2 cm and a diameter of 6 mm. The biochars were obtained at different process temperatures, stoichiometric oxygen ratios (λ) and steam-to-biomass ratios (SB). Detailed explanation of λ and SB is provided in **Supplementary Information – Section B**. Gasification tests were performed at atmospheric pressure. A summary of the parameters used during the production of the biochars is presented in Table 2. The biochars were labelled using the following format, BC_Test Number. For example, BC_1 stands for biochar produced from gasification test 1.

The four biochars were obtained from -air gasification tests (BC_1 and BC_2) and air/steam gasification tests (BC_3 and BC_4). Images of the biomass and biochars are shown in Fig. 1.

A schematic drawing of the IHBFBSR unit is presented in.

Fig. 2. The set-up is located at Delft University of Technology (TU Delft) and has been designed, built and commissioned by the Dutch company Petrogas Gas-Systems together with the Process & Energy Department of TU Delft.

The main components of the unit are: feeding system for biomass pellets (SB01, SB02 and SB03) and one for the additives (SB04); heating section composed by two preheaters (EH01 and EH02); the IHBFBSR unit; the gas cleaning unit composed by two cyclones in series (CYC01 and CYC02) and the gas analysis section composed by two main lines, one for the permanent gas online measurements and the other for the tar sampling.

The bed material employed in the experiments was corundum, which is mainly constituted from aluminium oxide and traces of iron oxide, titanium oxide and silica [25]. Corundum is typically used for its good heat distribution and extreme hardness, which limits attrition of the particles [25]. The corundum was provided by the company Unicorn ICS B.V and tests were performed considering two different grain sizes,[3] 590 μm (Bed_A) and 490 μm (Bed_B). Before each test 75 kg of corundum were introduced in the reactor. The bed material is typically considered inert.

Before starting a gasification test, the reactor was heated up till about 550 °C by the radiant tube burners and by feeding preheated nitrogen and air. Subsequently, a stoichiometric (λ = 1) combustion step (4 kg. h^{-1} of biomass and 22 kg.h^{-1} of air) was started with the aim of achieving average bed temperatures close to 850 °C. The average bed temperature was defined as the average values of thermocouples TE01 – TE05. Preliminary combustion tests performed in the IHBFBSR, showed that close to full conversion is achieved under the aforementioned conditions. Additionally, after the completion of the warming up step, the cyclones were emptied to avoid interference with the subsequent

[2] CGE = (mass flow rate•LHV) $_{product\ gas}$/(mass flow rate•LHV)$_{biomass}$ LHV = Low heating value.

[3] Weighted average value obtained from particle size distribution measurements (Supplementary Table E.1).

Table 1
Relevant studies addressing biochar generation through gasification in terms of feedstock and operating conditions.

Process conditions				Biochar				Ref
Gasifier type	Feedstock	Temperature (°C)	Agent	Yield[a] (%)	C (%)	Surface area (m^2/g^{-1})	Pore volume (cm^3/g^{-1})	
Downdraft	Wood chips	650, 800	–	–	–	183–427	0.25–0.39	[14]
Rising co-current	Wood pellets	700	–	–	–	403	0.50	[14]
BFB	Corn stover	700	Air	4.5	–	29	–	[10]
BFB	Corn stover	730	Air/N_2		38.5 (a.r.)[b]	23.9	–	[15]
BFB	Switchgrass	760	Air/N_2		42.8 (a.r.)[c]	31.4	–	[15]
BFB	Switchgrass	824	O_2/Steam	–	25.4 (a.r.)[b]	–	–	[16]
BFB	Residual wood	670	Air	–	82.0 (d.b.)[c]	217.0	0.1137	[17]
BFB	Beech wood	670	Air	–	77.0 (d.b.)[c]	86.0	0.0377	[17]
BFB	Greenhouse wastes	750	Air	–	59.0 (d.b)[c]	234.0	0.0431	[17]
CFB	Dry distiller's grain	780–830	O_2/Steam	0.7–3.1	–	22.5	–	[18]
CFB	Agrol	700–850	O_2/Steam	1.4–14.0	–	504.0–521.0	0.220–0.590	[18]
CFB	Willow	700–850	O_2/Steam	1.7–13.1	–	296.0–439.0	0.272–0.314	[18]
CFB	Straw	700–750	Air/Steam	4.0	45.5 (a.r.)[b]	75.0	0.040	[12]
TwoStage	Pine wood	1000–1200	Air/steam	4.0	52.0 (a.r.)[b]	426.0	0.520	[12]
Dual-stage	Wood chips	850–900	–	–	–	297.0–603.0	0.260–0.300	[14]
Plasma reactor	Wood pellets	700, 900	O_2	–	–	243–364	0.144–0.188	[19]

[a] Calculated as 100 – CC where CC in the carbon conversion efficiency.
[b] As received basis.
[c] Dry basis.

Table 2
Process production parameters of the investigated biochars (BC_1–4).

	BC_1	BC_2	BC_3	BC_4
Test	1	2	3	4
λ (−)	0.25	0.30	0.20	0.20
SB (−)	0.0	0.0	0.80	1.20
T (°C)[a]	850	850	836	840
Bed Material[b]	Bed_A	Bed_A	Bed_B	Bed_B

[a] Average bed temperature.
[b] Bed A: corundum with main diameter 590 μm. Bed_B: corundum with main diameter 490 μm.

measurements in the gasification phase. Once the desired temperature was reached, the biomass, air and steam flow rates were set and gasification started. Under the assumptions of this work, all the biomass converts into permanent and condensable gases, biochar and ash. It is considered that there is no unreacted biomass. The mass balance calculations assume that there is no biochar left from the combustion step and that all the biochar produced derives from 1 h of gasification at steady state (average data).

2.1.1. Quantification of biochar in the cyclones

During each test, ash together with fine biochar particles, were separated from the product gas by means of two cyclones. Each cyclone was connected to a bin where the ash and biochar were collected. The day after the test session, each bin was opened and its content (ash + biochar) was weighted and stored in a closed plastic bag. After mixing, two samples of 1 g each were taken, weighted and burned in a muffle furnace (Nabertherm 30–3000 °C) at 600 °C for four hours and then weighted again. The procedure was repeated till constant weight was reached (± 0.3 mg) as suggested by [26]. The difference between the last weight measurement and the initial weight of each sample was considered to be the biochar present in each sample before burning it. The average value obtained from the two samples was taken as the biochar lost with the ash in the cyclones. The detailed values obtained

Fig. 1. Biomass and biochars studied in this work. a) Biomass, b) BC_1 (T = 850 °C, λ = 0.25, SB = 0), c) BC_2 (T = 850 °C, λ = 0.30, SB = 0), d) BC_3 (T = 836 °C, λ = 0.20, SB = 0.80) and e) BC_4 (T = 840 °C, λ = 0.20, SB = 1.20).

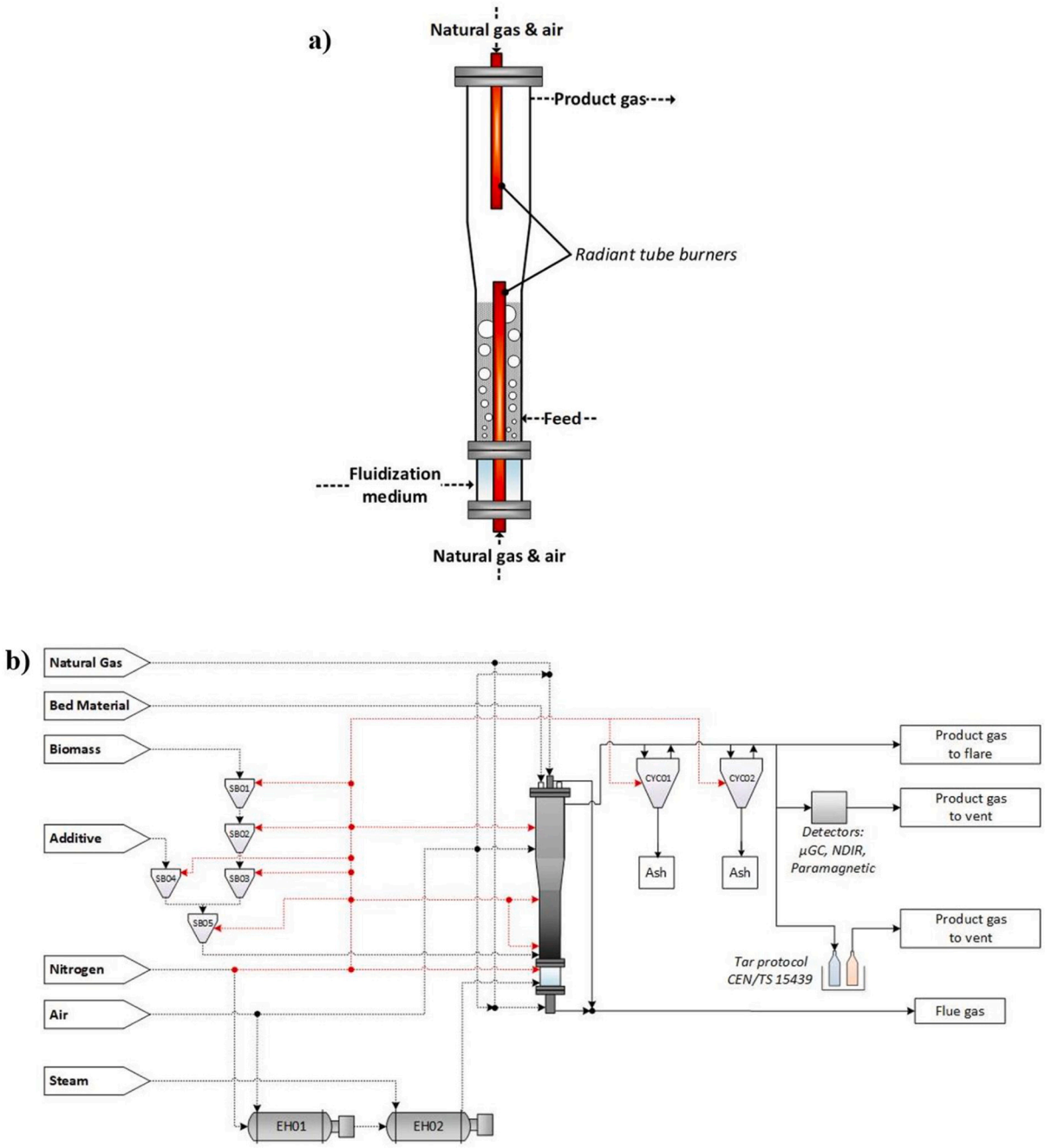

Fig. 2. Schematic drawing of the IHBFBSR gasification system. (a) IHBFBSR unit (b) entire setup including preheaters, reactor, gas cleaning unit and gas analysis section [21].

for this test are reported in Table 3.

2.1.2. *Quantification of biochar in the reactor*

After each gasification experiment, the reactor was cooled down in an inert (N_2) environment, emptied and the corundum and biochar were collected. The particle size distribution of the biochar collected from the reactor (Fig. 1) was determined using a sieve shaker (Retsch AS300), equipped with a tower of eight sieves of different mesh size (6000, 4750, 4000, 3500, 1400, 850, 600, 500 µm). Due to the similar size of the bed material and the biochar, it was not possible to collect biochar with a size smaller than 500 µm. The total bed material and biochar (< 500 µm) were firstly weighted and then 5 samples of 1 g each were combusted and weighted again. The procedure adopted for this quantification was the same explained in previous section. The average value obtained from the 5 samples was then taken as percentage of biochar (< 500 µm) lost in the bed. The detailed values obtained are reported in Table 3.

The total mass of the biochar (> 500 µm) collected after sieving was determined by gravimetric analysis and stored in a closed plastic bag. A sample of about 200 g was then taken from the bag, grinded with a Bosh MKM6000 and sieved with a 200 µm mesh size sieve. The biochar with a diameter smaller than 200 µm was recovered and stored in a closed plastic bottle of 250 ml and used for the characterization and surface analysis. The same procedure was applied to prepare the biomass sample. Results related to the amount of biochar produced from the different gasification tests and carbon conversion efficiency (CC) are presented in Section 3.1 **Gasification tests results: focus on solid streams**. Detailed explanation of CC is provided in **Supplementary Eq. C.1**.

Table 3
Gasification test results focusing on solid streams and considering 1 h of steady state except for the bed material. The bed material was loaded before each test.

Test	1	2	3	4
T (°C)	850	850	836	840
λ (−)	0.25	0.30	0.20	0.20
SB (−)	0	0	0.80	1.20
Biochar produced	BC_1	BC_2	BC_3	BC_4
Steady State (h)	1			
Bed Material	Bed_A	Bed_A	Bed_B	Bed_B
Biomass	Biomass			
IN				
Biomass in (kg)	13.9	11.6	10.0	10.0
Bed Material in (kg)*	75.0			
Tot IN (kg)	*88.9*	*86.6*	*85.0*	*85.0*
OUT				
Biochar sieved (kg)	0.08	0.07	0.12	0.23
Bed material + Biochar collected (kg)	73.51	73.62	74.73	73.57
Biochar <500 μm from Bed Material (wt%)	0.28	0.21	0.39	1.93
Biochar (< 500 μm) from Bed Material (kg)	0.05	0.05	0.04	0.27
Bed Material (kg)	73.46	73.57	74.69	73.30
Bed material + Biochar lost in the gasifier (kg)	1.54	1.43	0.31	1.71
Biochar (< 500 μm) lost in the gasifier (kg)	0.001	0.001	0.0002	0.01
Bed Material lost in the gasifier (kg)	1.54	1.43	0.31	1.70
Ash + Biochar collected (kg)	0.44	0.62	0.27	0.38
Biochar (< 500 μm) lost with the ash (wt%)	12.78	10.08	78.30	60.02
Biochar (< 500 μm) lost with the ash (kg)	0.06	0.06	0.21	0.23
Ash (kg)	0.39	0.55	0.06	0.15
Permanent and condensable gases**	13.32	10.86	9.57	9.12
Tot OUT (kg)	*89.9*	*86.6*	*85.0*	*85.0*
CC and Y_{BC_i} ***				
CC (%)	97.6	97.1	92.9	86.4
$Y_{BC\_i,tot}$ (%)	1.4	1.6	3.7	7.3
$Y_{BC\_i,net}$ (%)	0.6	0.6	1.2	2.3
$Y_{BC\_i,lost}$ (%)	0.8	1.0	2.5	5.0

* Loaded before each test. Bed material considered inert.
** Calculated by difference.
*** i refers to the gasification test considered.

2.2. Measurements and data analysis

Here we provide a description of the analytical techniques and experimental conditions applied in this study. The composition of biomass and biochar includes: major (>1% at.), minor (1–0.1% at.), and trace (<0.1% at.) elements.

2.2.1. Proximate and ultimate analysis

The Proximate Analysis was performed according to NREL/TP-510-42,621 [27] and NREL/TP-510-42,622 [26]. The moisture and ash content were determined using a convection drying oven and a Muffle Furnace (Nabertherm 30–3000 °C), respectively. The volatile matter was obtained with a thermogravimetric analyzer (TGA – SDT Q600). About 3 mg of each sample was initially introduced in an alumina pan and the temperature was increased from room temperature to 110 °C in nitrogen atmosphere (100 ml.min^{-1} at standard pressure) with a heating rate of 10 °C.min^{-1}. The reactor was kept isothermal for 10 min to ensure that the sample was dried. Afterwards, the sample was heated up to 600 °C with a heating rate of 10 °C.min^{-1} and maintained isothermal for 10 min to ensure sufficient decomposition process (pyrolysis). The weight loss in this step is defined as the amount of volatile matter included in the proximate analysis. The fixed carbon was then calculated by difference.

The Ultimate Analysis of all samples was conducted using a Euro-Vector EA3400 Series CHN-O analyzer with acetanilide as the reference. The oxygen content was determined by difference. All the measurements for the proximate and ultimate analysis were carried out in duplicate.

2.2.2. Higher heating value (HHV)

HHV was determined by using a bomb calorimeter (Parr 6772 Calorimetric Thermometer). The samples were introduced in the bomb in pellet shape, previously obtained by pressing about 1 g each of material in a hydraulic press. Each test was carried out in duplicate.

2.2.3. X-ray fluorescence (XRF)

XRF measurements were carried out with a Panalytical Axios Max WD-XRF spectrometer. About 2 g of biomass (in pellets form) were mixed with a cellulose/wax binder and pressed at a pressure between 15 and 35 T of pressure for 1–2 min prior analysis. The XRF spectra were collected with an energy resolution of 4 kW. Corrections for the binder were taken into account.

2.2.4. X-ray powder diffraction (XRD)

XRD measurements were performed with a Bruker D8 Advance diffractometer Bragg-Brentano geometry and Lynxeye position sensitive detector with a radiation source of Cu Kα (WL = 0.154 nm). About 100 mg of each sample were deposited as a thin layer on a Si510 zero-background-wafer fixed in PMMA holder LL510. The XRD pattern was recorded with a step size of 0.030 in 2θ, at 2 s per step, with a scan range of $10^{\circ} < 2\theta < 110^{\circ}$.

2.2.5. Scanning electron microscopy and energy dispersive X-ray spectroscopy (SEM-EDS)

Biochars were analyzed in low vacuum mode with a JEOL IT100 Scanning Electron Microscope (SEM) equipped with an Energy dispersive X-ray spectroscopy (EDS) detector. SEM images were recorded using a backscattered electron detector in a compositional mode with an accelerated voltage of 10 kV and beam current of 65 pA. The area of analysis was a few hundred micrometers and the depth about of 1 μm [28]. We examined two samples per each type of biochar and inspected two regions of interest (ROI) per sample to ensure a representative description of the biochars. For each ROI, we extracted a digital X-ray map and conducted a four-point scanning of the surface.

2.2.6. X-ray photoelectron spectroscopy (XPS)

Samples were prepared by placing about 10 mg of each material in a 1000 μl mixture composed by 50 μl of Nafion® perfluorinated resin solution and 950 μl of water and isopropanol in equal proportion. Nafion® is composed of a hydrophobic Teflon backbone coupled with SO_3H groups [29]. Then, the samples were sonicated for 1 h, deposited as a thin layer on a copper plate (1cm^3) and dried overnight. XPS analysis was carried out using a PHI-TFA XPS spectrometer (Physical Electronic Inc.), equipped with an x-ray Al-monochromatic source. The vacuum during XPS analysis was set to 10^{-9} mbar. The tested area was 0.4 mm in diameter and the analysis depth was 3–5 nm. High-resolution multiplex scans of the peaks were recorded using a pass energy of 23.5 eV with a step size 0.1 eV, at a take-off angle of 45° with respect to the sample surface. Low energy electron gun was used for surface charge neutralization XPS. Spectra were processed using Multipak v8.0 (Physical Electronics Inc.). High-energy resolution spectra of O1s and C 1 s photoelectron peaks were curve-fitted to quantify the relative amounts of O and C-based compounds at the surface of different biochars. Curve-fitting was carried out with a deconvolution of the oxygen peak into three components: O_2^-, OH^- and adsorbed H_2O and the carbon peak into the C-C/C-H, CO and COOX components [30].

2.2.7. Specific surface area (SSA), pore volume (PV) and pore size distribution (PSD)

N_2-physisorption tests were performed on a NOVAtouch™-LX gas sorption analyzer from Quantachrome Instruments with high purity N_2 (99.99%) at 77 K. Prior to the measurements, the samples were vacuum degassed at 130 °C for 16 h. Each test was performed in duplicate. SSA was calculated by applying the The Brunauer-Emmett- Teller (BET) theory and particular size distributions were obtained at the same time

from the isotherms based on Quenched-Solid Density Functional Theory (QSDFT). Adsorption branches (relative pressure, $P{\cdot}P_0^{-1}$, in the range between 0.05 and 0.20) were used to determine the SSA. PV was obtained from the amount of N_2 adsorbed at $P{\cdot}P_0^{-1} = 0.95$. Results are presented in Fig. 10 (N_2-physisorption isotherms), Fig. 11 (PSD curves) and Table 7 (SSA and PV).

3. Results and discussion

3.1. Gasification tests results: focus on solid streams

Table 3 summarizes the results obtained for the four gasification tests. The solid streams comprise the bed material, bed material losses (in the gasifier), useful biochar for further applications (recovered from sieving the bed material and biochar, > 500 μm) and biochar losses (< 500 μm in the bed material, gasifier and ash in the cyclones). Additional information, and mass flow diagrams of the gasification tests performed can be found in Supplementary Information - Section C.

The biochar yield produced by the IHBFBSR gasification system is comparable to other gasification units. For example, [12] report biochar yields of 4% and 10% for a TwoStage gasifier and Low Temperature Circulating Fluidized bed gasifier, respectively. Similarly, [31,32] report a biochar yield of 10% (db) for tests carried out in a fixed-bed downdraft gasifier between 600 and 700 °C.

Only a small difference is observed in the biochar yield between air gasification tests (Table 3), even when λ increases from 0.25 (Test 1) to 0.30 (Test 2). Nevertheless, when compared to air/steam gasification and literature data [15], air gasification, Test 1 and Test 2, produces very low amount of biochar, 1.4% and 1.6% of the feedstock mass, respectively. This is partly attributed to the influence of the equivalence ratio λ. In fluidized bed gasification, λ is linked to the oxygen availability and usually varies between 0.2 and 0.4 [33]. The lower values of λ used in air/steam gasification tests translate into a lower oxygen availability so the combustible gases and the biochar in the gasifier react less. This leads to an increase of the biochar mass yield as well of its carbon content [34]. The difference between the obtained total biochar yields ($Y_{BC,i,tot}$) of 0.2% reported between Test 1 (BC_1) and Test 2 (BC_2) is mostly attributed to the biochar lost in the cyclones with the ash.

For air/steam gasification tests, the effect of λ is coupled with the influence of SB. In general, the introduction of steam leads to the promotion of the Water Gas reaction[4], therefore higher carbon conversion efficiency (CC) would be expected at increasing SB [35]. At the same time, at constant biomass and air flow rates, the introduction of more steam leads to an increase of the fluidization velocity and, consequently, to a reduction of the gas resident time which translate to less CC. Moreover, a lower CC is also linked to the bed temperature drop due to the introduction in the reactor of steam at lower temperature compared to the operating one [36]. The results presented in Table 3 are in agreement with these two last points. They show a decrease of CC of 6.5% going from SB = 0.8 (Test 3) to SB = 1.2 (Test 4) where the lowest CC value among the four tests is found (CC =86.4%). In the IHBFBSR the above-mentioned drop in the bed temperature is not directly seen by the temperature reading (Table 2) because the reactor works according to a set point. However, in our previous study [21], we found that for lower SB, the operating time of the bottom burner was lower, meaning that the heat requirement of the process was reduced. In other words, the introduction of more steam, reduces the CC and leaves more carbon available for the oxidation reactions reducing the heat requirement of the process. These results are also confirmed by the total biochar yield obtained: the value decreases from 7.3.% in Test 4 ($Y_{BC,4,tot}$) to 3.7% in Test 3 ($Y_{BC,3,tot}$), while the SB value decreases from 1.20 to 0.8.

[4] $C + H_2O \leftrightarrow CO + H_2$.

3.2. Particle size distribution

Fig. 3 presents the particle size distribution of the biochars obtained from each gasification test.

Fig. 3 shows that the studied biochars have a high weight percentage of particles smaller than 500 μm. At laboratory stage, the biochar in this sieve range (<500 μm), is not directly available for further use as it is still mixed with bed material collected from the gasifier, with the ash from the cyclones or it remained in the reactor with the bed material that could not be collected (See Table 3-). These findings provide valuable insight regarding the type of particles entrained in syngas and serve as guidance for selection of downstream equipment and handling systems. In case of a continuous process, however, the bed material and the fine biochar (<500 μm) could be combusted to generate process steam.

In general, the useful fraction of the biochars contains particles mainly in the range between 1400 and 3500 μm (Fig. 3). For lower size steps, air gasification biochars (Test 1 and Test 2) have higher weight percentages in the range between 800 and 1400 μm, while for air/steam gasification biochars (Test 3 and Test 4) the particles are more equally distributed in the three ranges between 600 and 1400 μm. For higher size steps (4000–6000 μm) biochar weight percentages decrease with the increase of λ (Test 1 and Test 2) and with the increase of SB (Test 3 and Test 4).

Results indicate that the amount of biochar that can be separated from the bed material is higher in case of air gasification, reaching the highest value of 46% in Test 1 (Fig. 3). In Test 2, instead, the increase of the amount of air, from λ = 0.25 to 0.30, translates into a value that is 10% lower compared to the one obtained from Test 1 (Fig. 3). In case of air/steam gasification (Test 3 and Test 4), the biochar directly separated from the corundum decreases even more as compared to Test 2 (3% for Test 3 and 5% for Test 4). The two tests, however, have very similar values (33% for Test 3 and 31% for Test 4).

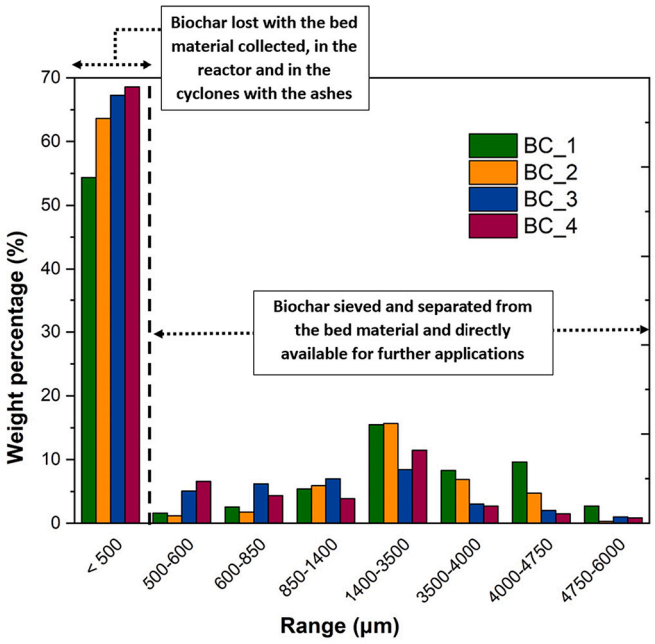

Fig. 3. Particle size distribution of biochars BC_1–4 obtained after emptying the reactor. Green color, orange color, blue color and violet color represent BC_1 (T = 850 °C, λ = 0.25, SB = 0), BC_2 (T = 850 °C, λ = 0.30, SB = 0), BC_3 (T = 836 °C, λ = 0.20, SB = 0.80) and BC_4 (T = 840 °C, λ = 0.20, SB = 1.20), respectively. (For interpretation of the references to color in this figure legend, the reader is referred to the web version of this article.)

3.3. Proximate, ultimate analysis and high heating values

Table 4 presents the results of the Proximate and Ultimate Analysis of the parent biomass and biochars. The O/C, H/C, C/N molar ratios and high heating values (HHV) are also included in Table 4.

Regardless of the process conditions, the biochars produced by the IHBFBSR unit are classified as carbon rich, with a carbon content in the range of 92–96% (Table 4). The carbon content of all samples is compliant with the "European Biochar Certificate" (EBC), which requires a carbon content higher than 50% [37]. Our findings also support the hypothesis of Fryda and Visser [17], who suggested that carbon enrichment of woody biochars is partly due to the low ash content of the parent feedstock. All studied biochars have relatively low ash content but some differences are still observed between them, if grouped by gasifying agent (Table 4). In average, the ash content of air gasification (BC_1, BC_2) and air/steam biochars (BC_3, BC_4) increased 13 and 7 times compared to the parent biomass. The ash content of air gasification biochars is two-fold higher compared to air/steam gasification ones. These findings support our hypothesis that an oxygen-rich environment promotes combustion reactions converting more carbon into volatiles/syngas, while increasing the ash fraction due to accumulation of inorganic constituents (Table 4, Proximate Analysis). Similar behavior has been reported in [19]. Biochars with high fixed carbon content are considered high quality [34]. Hence, BC_4 has the highest quality of the studied samples.

The influence of the process conditions on the elemental composition of the studied biochars is presented in the Van Krevelen diagram (Fig. 4-). The diagram presents the H/C molar ratio as function of O/C molar ratio of the studied biomass and biochars BC_1, BC_2, BC_3 and BC_4. The values for H/C and O/C ratio can be found in Table 4.

Fig. 4- shows that the parent biomass belongs to the position of woody biomass [39]. The studied biochars present O/C (0.02–0.04) and H/C (0.09–0.19) molar ratios in the anthracite range, resulting in a higher heating value compared to the parent biomass (Table 4). These ratios, comparable with the values reported from literature (Fig. 4-) for gasification derived woody biochars, meet the requirements of the EBC, which mandate an O/C and H/C atomic ratio lower than 0.4 and 0.7, respectively [37].

Table 4
Proximate and CHNS Elemental analysis of the biochars BC_1, BC_2, BC_3, BC_4 and biomass, corresponding molar ratios of O/C, H/C and C/N and high heating values (HHV).

Proximate analysis (wt% a.r.[a])					
	Biomass	BC_1	BC_2	BC_3	BC_4
Moisture	5.08	4.53	3.87	1.42	1.86
Fixed Carbon	18.63	82.11	84.52	91.80	92.18
Volatile Matter	75.60	3.56	3.22	1.89	1.82
Ash	0.69	9.80	8.39	4.89	4.14
CHNS Elemental Analysis (wt% d.a.f.[b])					
C	48.76	92.47	94.36	96.06	93.02
H	6.06	1.49	1.48	0.76	0.86
O[c]	44.86	5.31	3.48	2.37	5.47
N	0.30	0.55	0.62	0.53	0.45
S	0.01	0.17	0.06	0.27	0.20
Molar ratios					
O/C	0.69	0.04	0.03	0.02	0.04
H/C	1.48	0.19	0.19	0.09	0.11
C/N	189.54	196.07	177.49	211.36	241.06
High heating values (MJ.kg^{-1} a.r.[a])					
HHV	18.89	28.14	29.20	31.28	30.60

[a] As received basis.
[b] Dry ash free basis.
[c] Calculated by difference.

BC_3, produced at the lowest gasification temperature (836 °C) indicates a higher release of H and O, and retention of C compared to other investigated biochars. Yet, all biochars are grouped in the low left corner of the Van Krevelen diagram (Fig. 4). According to Spokas classification [40], all biochars (BC_1–4) are highly stable with a half-life higher than 1000 years, since their O/C is <0.2. Biochars with a high percentage of stable carbon compared to the parent biomass are known to have a high carbon sequestration potential due to its resistance against degradation reducing C emissions to the atmosphere [41,42].

Based on Fig. 4, the O/C ratios found for the literature biochars are in the range between 0.05 and 0.31, higher compared to the results obtained for our biochar (0.002–0.004). These O/C values suggest that our biochars present a higher degree of carbonization, high aromaticity and low polarity compared to the literature woody gasification derived biochars [43]. This could be attributed to the high temperature of the IHBFBSR unit compared to the temperatures considered from literature (600–800C).

Similar results were also found in [17,43]. The first reference report O/C ratios between 0.01 and 0.10 at 650 °C while the second reference reports O/C ratios in the range of 0.003–0.19 for gasification temperatures between 400 °C–750 °C. The studied biochars also have a half-life ten times larger than the duration normally considered in life cycle assessments to calculate the global warming potential [44]. Thus, the contribution of its decay to the long term GHG balance is relatively small [13]. In regards to H/C ratio, biochars with such low content of hydrogen and oxygen are typically highly aromatic which could result in improved hydrophobicity [45]. The C/N molar ratio (Table 4) provides a more accurate picture regarding the effect of the gasification agent. Higher C/N values are obtained for BC_3 and BC_4 compared to BC_1 and BC_2, which might be related to the influence of λ. Higher values of λ for air gasification (Table 2**:** BC_1 = 0.25, BC_2 = 0.30) compared to steam gasification samples (Table 2: BC_3, BC_4 = 0.20) led to higher concentration of N on BC_1 and BC_2. If used as soil amendment, our biochars might lead to N immobilization since the C/N ratio of all studied biochars is higher than 30 [46], typically of woody biomass [47]. Although other studies [47,48] indicate that a biochars with high C/N ratio reduce N availability and thus increase the potential for adsorption of NH_4^+, which translates into reduced N leaching and higher N fertilization over time, especially in surface soils. Further, N immobilization can be expected to be negligible when C-rich biochars are used in soil due to the small fraction of the labile C-pool and the recalcitrance of the remaining biochar-C, after initial mineralization of fresh biochar [49]. Thus, further research should focus on gasification biochar-soil interactions, as it is known that N immobilization not only depends on the C/N of biochar but also on the C/N of the soil [50].

3.4. XRF

The oxide composition of the inorganic compounds of biomass and biochars was determined by XRF analysis and is presented in Table 5. Oxides detected with a wt% lower than 0.01% can be found in **Supplementary Table F.1**. The XRF measurements of the bed material can be found in **Supplementary Table F.2**.

Regardless of the process conditions, almost all the compounds present in the parent biomass, except for Cl and Na_2O, are enriched in the studied biochars. Minerals like calcium, potassium, phosphorus and magnesium, are expected to increase and accumulate on the biochar surface as ash [51]. This is attributed to the volatilization of the organic structure (C, H and O), vaporization temperature of inorganic constituents and deposition of corundum. Alkali and alkali earth metals (AAEM), especially calcium and potassium, are known to increase biochar pH [51] or act as catalysts enhancing biochar reactivity in gasification in CO_2 [34]. Bed material deposition on biochar was also reported by Meng [18]. This hypothesis is backed by the fact that all constituents that are found in high quantities in the biochars and not in the biomass are also present in the corundum, e.g., Al_2O_3 (**Supplementary**

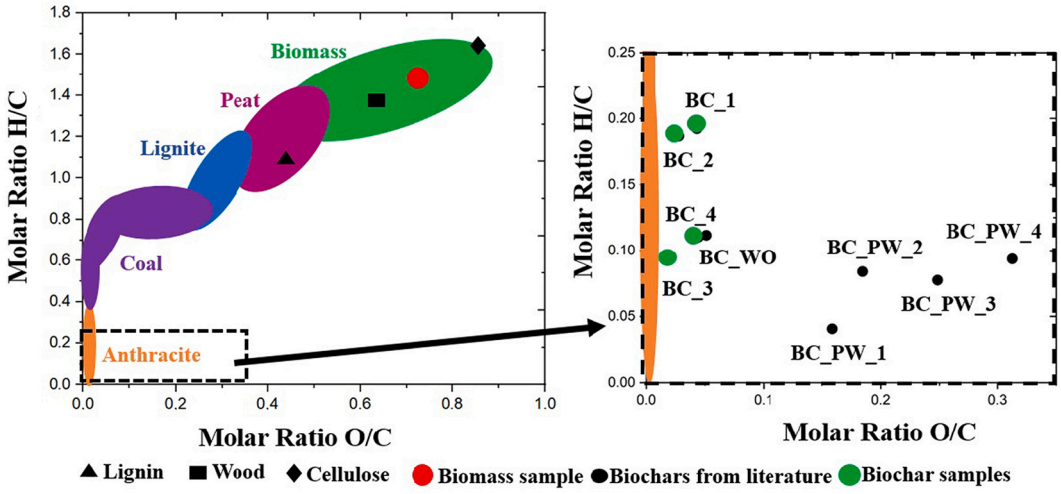

Fig. 4. Van Krevelen diagram of studied biomass and biochars (BC_1–4). Other biochar data were reported by [38]. The literature biochars considered were produced from wood gasification in the temperature range of 600–800 °C, PW = pine wood and WO = white oak. This figure has been adapted from [39]. Red circle indicates the studied biomass and multiple green dots represent the studied biochars. The values for H/C and O/C ratio for the biochars studied can be found in Table 4. (For interpretation of the references to color in this figure legend, the reader is referred to the web version of this article.)

Table 5
XRF measurements of the inorganic constituents of the biomass and biochars (BC_1–4).

Compound	wt% a.r.				
	Biomass	BC_1	BC_2	BC_3	BC_4
$C_6H_{12}O_5$	99.353	–	–	–	–
C (balancing compound)	–	96.124	97.182	97.458	97.046
CaO	0.119	1.184	1.022	1.167	1.421
K_2O	0.028	0.460	0.442	0.122	0.191
Al_2O_3	0.125	0.572	0.373	0.188	0.169
SiO_2	0.204	0.571	0.299	0.38	0.396
MgO	0.043	0.370	0.256	0.303	0.331
Fe_2O_3	0.019	0.090	0.077	0.094	0.119
P_2O_5	0.01	0.173	0.069	0.087	0.096
SO_3	0.021	0.087	0.067	0.062	0.069
TiO_2	0.013	0.077	0.058	0.072	0.082
Na_2O	0.039	0.198	0.050	–	–
MnO	0.005	0.033	0.029	0.032	0.042
Cl	0.017	0.033	0.026	0.015	0.018

Table F.2). The highest concentration of Al_2O_3 was detected in BC_1. More information about corundum deposition is presented in **Supplementary Information - Section G**.

Table 5 shows that Na_2O is present only in BC_1 and BC_2. This suggests that Na-compounds were evaporated under air/steam gasification process conditions. Devolatilization of Na_2O was higher than K_2O, which could be attributed to the formation and stability of K-aluminosilicates compared to Na-aluminosilicates [52]. Devolatilization of AAEM during gasification is well documented in literature [38] and can lead to the formation of agglomerations and fouling, especially in the presence of Cl [33]. Fouling, slagging and corrosion can also be caused during combustion of biochars that contain CaO, MgO and Fe_2O_3 [53].

Furthermore, detailed results (**Supplementary Table F.1**) indicate the presence of traces of heavy metals in the form of oxides in our biochars: PbO (<0.003, except for BC_2 and BC_3), CuO (< 0.008), ZnO (<0.02) and Cr_2O_3 (<0.008). Further research is required to provide guidance about the influence of these elements for future applications. Nevertheless, it is known that biochar binds effectively to a number of heavy metals, immobilizing them for a long time [37]. In case the studied biochars are used in agriculture, toxic accumulation of heavy metals could be neglected, due to the low quantities of biochar used in this application [37].

3.5. XRD

XRD was used to complement the results obtained from XRF. Fig. 5 shows the XRD spectra of biomass and biochars BC_1–4.

Two broad peaks are observed at 2θ = 17 and 23 for raw biomass, which is attributed to cellulose and turbostratic crystalline C, respectively [54]. As expected, the XRD pattern of the parent biomass (Fig. 5a) confirms the presence of SiO_2, which is in agreement with the results obtained from XRF measurements (Table 5).

From Fig. 5 (b-e) it is seen that all investigated biochars have analogous patterns in which three main broad peaks ($10 < 2\theta < 35$; $40 < 2\theta < 60$; $75 < 2\theta < 90$) are recognized over the 2θ range. These peaks are typical of graphite [55]. After gasification, all studied biochars contained residual cellulose (2θ = 17) which indicates that not all the cellulose reacted during biochar formation. Based on the intensity of the crystalline C signal provided in Fig. 5, the studied biochars are ranked as follows: BC_3 > BC_2 > BC_4 > BC_1. Moreover, sharp peaks marked with blue (Al_2O_3), red (SiO_2) and green (Ti_2O) in Fig. 5 (b-e), confirm corundum deposition on the surface of all studied biochars since Al_2O_3, Ti_2O and SiO_2 are the main constituents of corundum (**Supplementary Table F.2**). The sharp peaks represent crystalline phases with high degree of long order [55]. In addition to these three crystalline phases (Al_2O_3, Ti_2O and SiO_2, also $Ca(OH)_2$ and $CaCO_3$ are present in all the four biochars. This is consistent with the high Ca content of the biochars (Table 5).

3.6. SEM-EDS

Fig. 6 presents details about the morphology and elemental analysis of the major (> 1% at.) and minor (0.1–1% at.) elements detected at the surface of each biochar. Results are presented in a grid of 8 columns and 4 rows, where the first columns show images of the biochars at 100× magnification, followed by 16 EDS maps. Detailed elemental concentrations of EDS maps are provided in **Supplementary Table G.1**. Microstructure of the biochars is presented in detail in **Supplementary Fig. G.1**.

The morphology of the biochars is in agreement with particle size distribution measurements (Fig. 3). From SEM images it is observed that air/steam gasification biochars have a lamellar structure with a larger porous pattern compared to air gasification samples (**Supplementary Fig. G.1**). This is attributed to the high volatile matter of the parent biomass [56], reactivity of O_2 [57] and the kinetic diameter of the H_2O

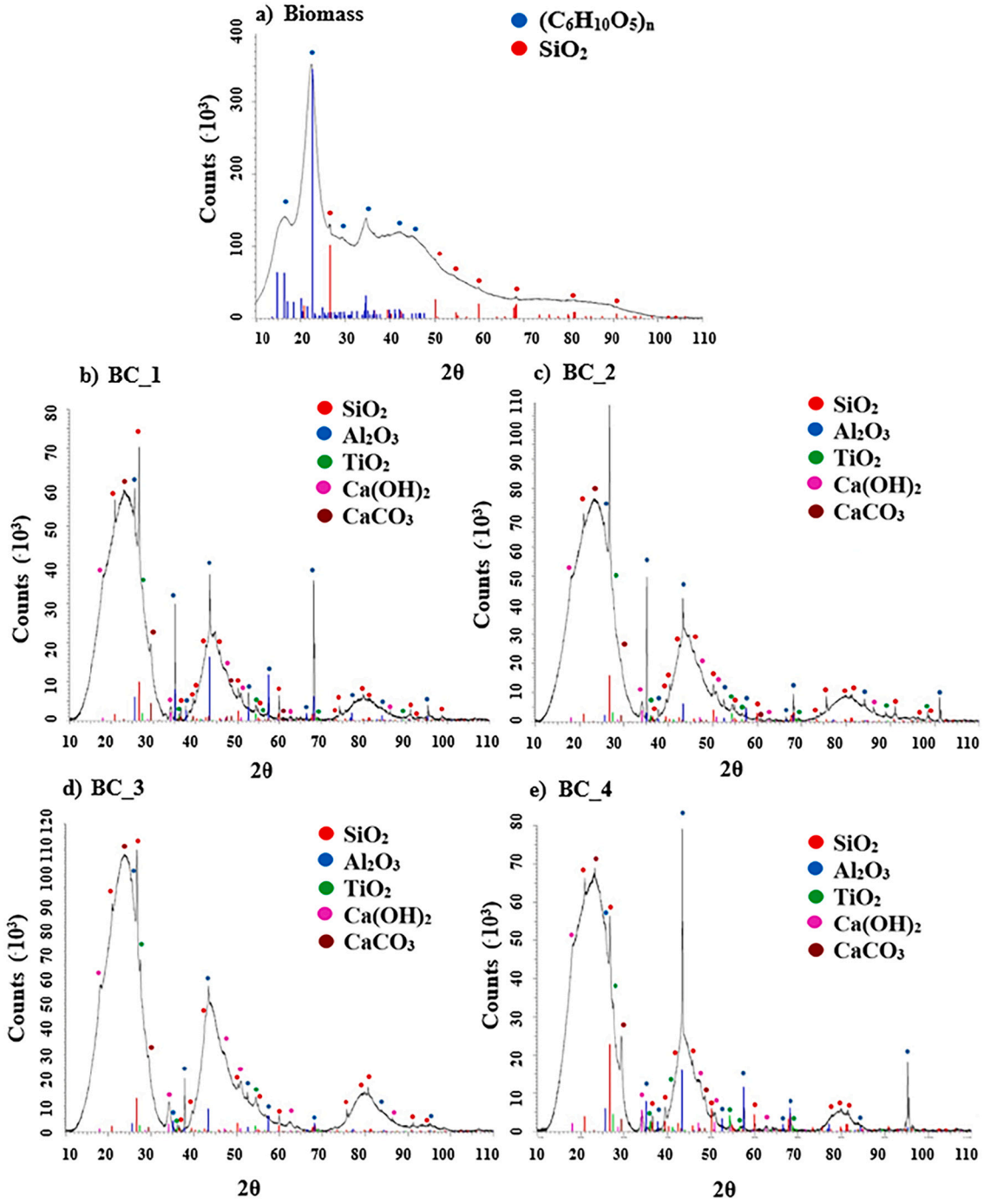

Fig. 5. XRD spectra of biomass and biochars BC_1–4.

molecule. Biochars produced in an O_2 environment are associated with high-burn off and poor development of the porous structure (macropores) [57]. Meanwhile in air/steam conditions, the kinetic diameter of the H_2O molecule is smaller than O_2 (265 and 345 pm, respectively [58]) and when diffusing through the surface of biochar penetrates longer and upon reaction creates a larger porous pattern. Our findings are in line with the recent evidence, which indicates that gasification using air/steam produces biochars with similar characteristics of activated carbons with high specific surface areas and total pore volume [38]. A larger porous structure increases the retention of nutrients, water [45] and reactivity of the biochar surface [59], which is beneficial for its use as soil amendment or CO_2 adsorbent [12]. A higher reactivity is also expected from air/steam gasification samples due to the fact that biochars contain less ash than air gasification ones (Table 4). This suggests less ash partially filling or occupying the pores and likely blocking reaction sites at the surface of the biochars [12]. This is supported by results from proximate analysis (Table 4). In general, despite the high temperature of the gasifier (850 °C) compared to some other thermochemical processes, SEM images indicate no sign of pore clogging.

From EDS SEM micrographs (Fig. 6) it is observed that in average, the surface of biochars contains several elements such as C > O > Al > Ca > K > Si > Mg > Na. The average surface O/C ratio (Supplementary Table G.1) of the biochars is comparable to low volatile bituminous coal [40] and follows the same trend reported by CHNS analysis (Table 4). In average, surface elemental analysis indicates that the samples produced from air gasification (BC_1 and BC_2) have in average a higher content of

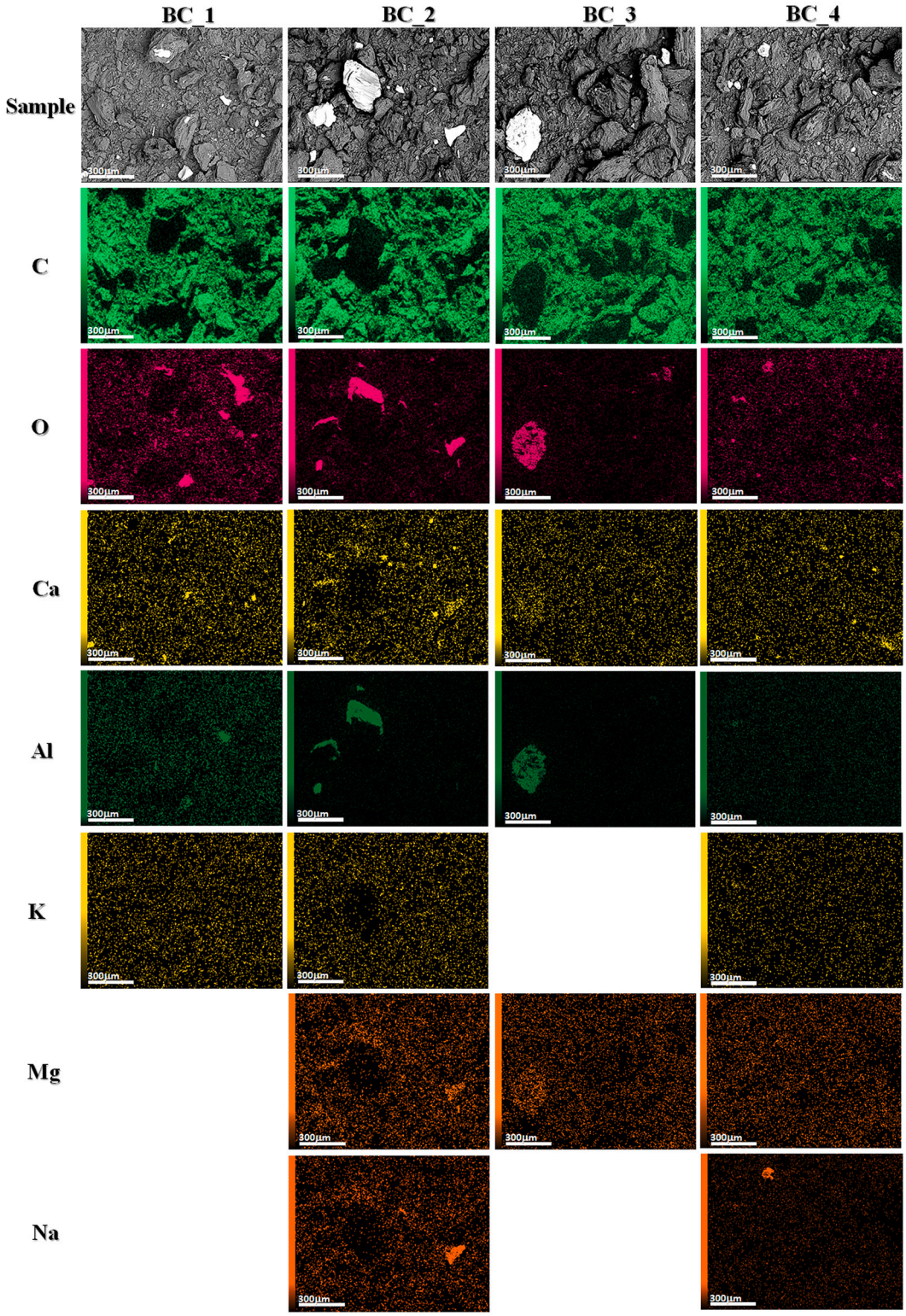

Fig. 6. EDS maps of major (> 1% at.) and minor (0.1–1% at.) elements located at the surface of the biochars. Each sample is ordered from top to bottom in the rows: BC_1, BC_2, BC_3 and BC_4. Elements are ordered from left to right in the columns: C, O, Ca, Al, K, Mg and Na. Coloured signals in each map indicates the presence of an element. Empty maps mean that the element was not detected at the surface of the sample. Detailed elemental concentrations of EDS maps are provided in **Supplementary Table G.1.**

Al and O compared to air/steam gasification biochars. Gasification at 840 °C produced the biochar (BC_4) with the lowest bed material (Al content) compared to other studied biochars (Fig. 6 and **Supplementary Table G.1**). The Al detected in the EDS SEM micrographs (Fig. 6) is most likely due to the bed material used during gasification, which is too small (< 500 µm) to be separated by sieving. This is observed on SEM images (Fig. 6), where a corundum grain is observed at the surface of BC_2 and BC_3. This observation is also backed by EDS elemental concentrations reported on **Supplementary Table G.1** and XRD results presented on Fig. 5. The bright color of corundum, especially on BC_3

surface, indicates little interaction between the alkali and alkali earth metals (AAEM) of the biochar and the bed material. Meanwhile in BC_2 some AAEM-based elements of the biochar are detected at the surface of corundum, which indicates some chemical interaction. Ca-compounds from gasified chars are known to interact with corundum to form aluminosilicates [60,61], which explains the reduced average CaO content in BC_2 compared to all biochars.

In general, all studied biochars have a uniform distribution of Ca and K (except BC_3) on their surface. SEM images of BC_2 also suggest the occurrence of chemical reactions between Ca -containing constituents of biochar and bed material during the gasification process. Based on XRD analysis, Ca-containing constituents at the surface of BC_2 are likely in the form of $CaCO_3$ and $Ca(OH)_2$ (Fig. 5). K- and Na-containing traces are also observed at the surface of BC_2, which are of relevance if biochar is used for combustion processes. Na and K are dominant elements responsible for slagging and fouling [62]. Contrary to coal gasification [60], SEM-EDS results suggest that low surface Si/Al ratios (**Supplementary Table G.1**) increase the ability of biochar AAEM species to stick to the surface of the bed material. Nevertheless, the quantities of AAEM-based elements observed at microstructure of corundum especially on BC_2 is so small that no significant influence is expected in large scale gasification. Furthermore, EDS SEM micrographs show no agglomeration of bed particles at the studied conditions for any of the gasification environments nor indication of erosion of the reactor walls. The presence of bed material in the biochars is also attributed to the sieving method which could not separate particles smaller than 500 μm.

3.7. XPS

The composition in the near-surface region and the oxidation state of elements present at the surface of biochars were determined by XPS analysis. Table 6 shows a qualitative comparison of the surface chemical composition for the different biochars, as obtained from XPS survey spectra (**Supplementary Fig. H.1**). F is present as a major element at the surface of all biochars result of sample preparation with Nafion (see Section 2.2 **Measurements and Data Analysis**).

At the near-surface region, no clear trend is observed between air and air/steam gasification tests regarding elemental composition of biochars. In average, air gasification leads to a decrease in C and O content on the biochar surface, while steam gasification reports a decrease in C content and increase in O content. Detection of C is attributed to the composition of the parent biomass and the presence of ambient contamination, typically involved in surface analysis [63]. The detection of O is related to the oxide layer formed on the surface of the biochar or of the entire particle. This is observed in the air gasification tests, where a decrease in the O content is related to less oxides in the entire particles of biochar, shown by XRF (Table 5**)**. The O/C ratio of the near-surface region for the studied biomass and biochars is higher than the values reported by Ultimate Analysis (Fig. 4) and SEM-EDS (**Supplementary Table G.1**). This is attributed to the presence of F in Nafion, used during sample preparation, which is present in a high amount masking deeper carbon-based regions inaccessible with XPS beam [64]. Nevertheless, XPS results indicate that gasification decreased active oxygen-containing groups on the surface of biochars compared to those of the parent biomass.

Minor amounts of Cu, S and Si are observed on the surface of all biochars BC_1–4. These elements are related to plant growth, harvesting, transport and processing of the parent biomass (Cu, S, Si) and bed material (Si). BC_3 indicates a highest concentration of Al (10.5%) on all samples. This is attributed to the bed material to be elaborated further with XPS high resolution spectra. BC_3 also contains significant amounts of Cu, S, Si and Na compared to the rest of the samples, which are also attributed to corundum. These results are in accordance with EDS measurements presented in **Supplementary Table G.1**).

The oxidation states of different elements at the surface of the biochars were determined by the high-resolution spectra. O 1 s and C 1 s spectra were curve fitted, whilst Al 2p, Cu 2p, S 2p, Si 2p, Ca 2p, Na 1 s and N 1 s were described only qualitatively. The O 1 s spectra can be separated into three component peaks: oxide, O^{2-}, at approx. 530 eV, hydroxide, OH^-, at approx. 531 eV, and water/carbonate, H_2O/CO_x, at approx. 533 eV [65]. Deconvolution of the peak O 1 s of different biochars is presented in Fig. 7 and the percentage of each component peak in Table 6.

Fig. 8 presents the C1s spectra deconvoluted into four sub-peaks CF_3 (approx. 293–294 eV), CF_2 (approx. 291-292 eV), due to the Nafion and COO (approx. 288–286 eV) and C-C/ C-H (approx. 286–284 eV) [67,68]. Since CF_3 and CF_2 peaks result from Nafion, which was used for XPS samples' preparation, they will not be part of the interpretation. Detailed areas (expressed as %) of the individual peaks can be found in Supplementary Table H1.

The results show that air/steam gasification biochars (BC_3 and BC_4) have the highest fraction of C-C/C-H functional groups of all studied samples. These results are in agreement with XPS results reported in [69], where high abundance of C-C/C-H functional groups are typically found in the near-surface of gasification biochars. C–C bonds are quite stable [70], which make them more resistant to degradation compared to biochars with higher O^{2-} such as BC_1 > BC_2. Our results also follow the same trend reported in the Proximate and Ultimate Analysis (Table 4) regarding the high aromaticity of BC_3 and BC_4. On the contrary, O-containing functional groups (O=C-O) are present in a higher percentage in air gasification biochars mainly due to the higher λ used in gasification tests compared to air/steam experiments (Table 2). The aromatic C=C and aliphatic C—C bonds are challenging to differentiate in Fig. 8 due the close proximity of their intensity peaks.

Fig. 9 presents the non-normalized high-resolution spectra of C 1 s, Al 2p, Cu 2p, S 2p, Si 2p and N 1 s.

Carbon is present on all studied biochars (Table 6), but peak C 1 s is more intense in BC_2 and especially in BC_4 (Fig. 9). The C-based layer on BC_2 and BC_4 is dominant on the surface and oxides/hydroxides are likely to be present beyond the near surface region. In BC_1 and BC_3, the intensity of C 1 s is lower due to the higher propotion of oxide/hydroxides at the near-surface region. On BC_3 a clear peak of Al 2p is noticed and confirms the erosion of corundum and deposition of corundum-based particles at the near-surface of the biochar. **Fig. 9**b findings back up result from XRF (Table 5) and SEM-EDS (Table 6) analysis that BC_3 contains higher amounts of Al-based compounds compared to the other studied biochars. Cu 2p, S 2p, Si 2p and N 1are detected on BC_3 and BC_1 (Fig. 9c), while on BC_3 their amounts are higher. This confirms our hypothesis that C 1 s covers oxides/hydroxides on the surface of BC_2 and BC_4, since Cu 2p, S 2p, Si 2p and N 1 s are not

Table 6
Elemental surface composition of different samples of biochar obtained from Survey XPS spectra.

Sample	C	O	Al	Cu	S	Si	Ca	Na	N	F	K	O/C
	(at.%)	(at.%)	(at.%)	(at.%)	(at.%)	(at.%)	(at.%)	(at.%)	(at.%)	(at.%)	(at.)%	(at.%)
Biomass	32.4	12.7	–	–	–	–	0.4	1.4	–	50.4	2.7	0.4
BC_1	36.2	5.4	3.5	0.7	0.4	0.4	0.1	–	–	53.3	–	0.2
BC_2	29.4	3.9	1.3	0.4	0.1	0.2	0.1	0.8	–	63.8	–	0.1
BC_3	32.2	7.4	10.5	1.9	1.1	0.8	0.1	1.6	0.1	44.3	–	0.2
BC_4	30.8	7.5	1.4	0.7	0.9	0.3	–	–	0.3	58.1	–	0.2

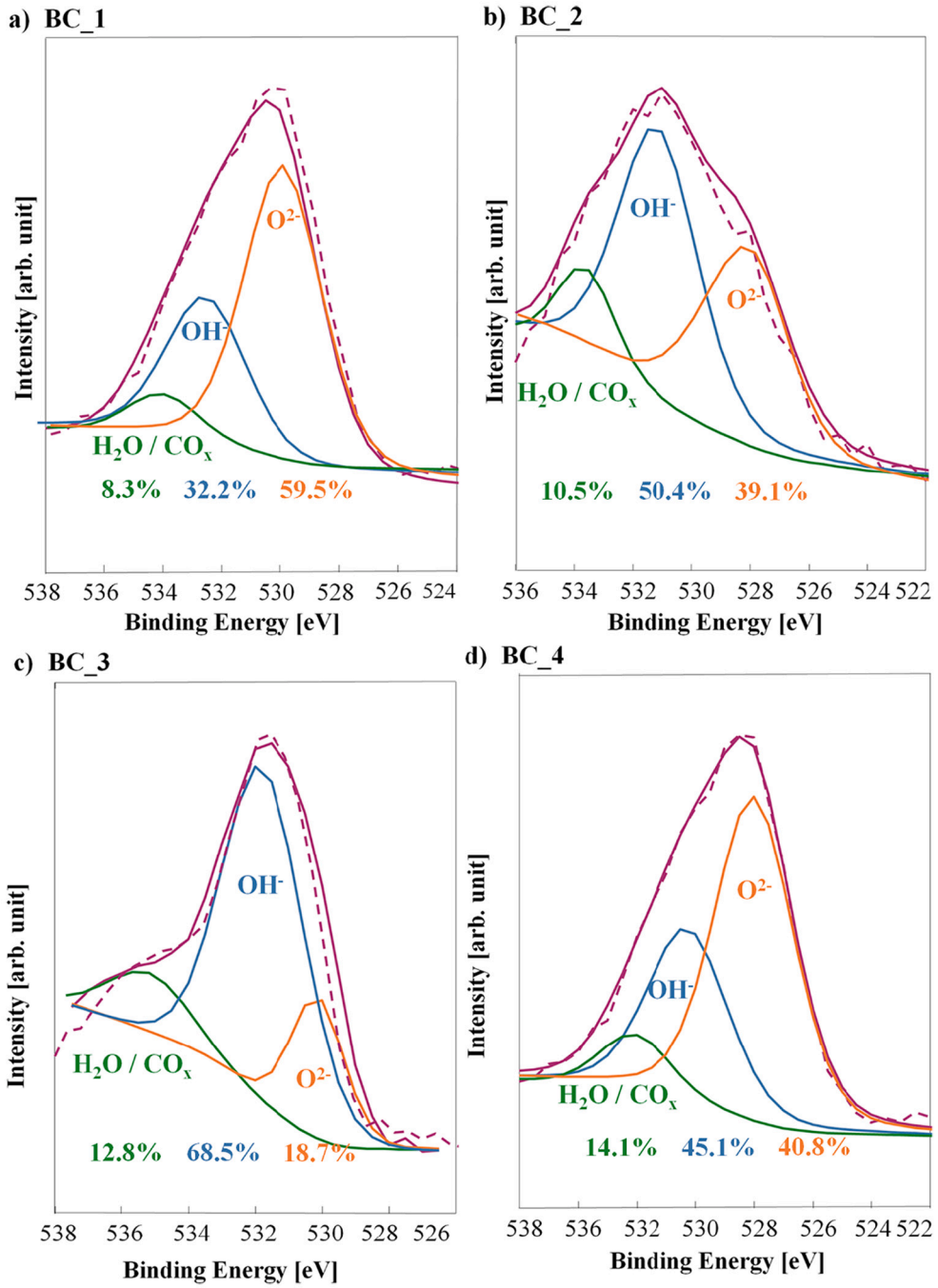

Fig. 7. High resolution spectra of O 1 s recorded on biochars BC_1–4. Purple solid line denotes experimental data and dotted its fit after deconvolution of H_2O/CO_x (green line), OH^- (blue line) and O^{2-} (orange line). (For interpretation of the references to color in this figure legend, the reader is referred to the web version of this article.)

detected. Fig. 9 confirms that air/steam gasification at 836 °C significantly affects the morphology, microstructure and chemical bonding (BC_3). Further study would be required to corroborate further differentiation between the oxidation state of each element.

3.8. SSA, PV and PPS

Fig. 10 presents the results of the N_2-physisorpion tests performed at 77 K of the biomass and biochars (BC_1–4) investigated in this work.

The isotherms of all the investigated biochars (**Figs. 10**b, c, d and e) are representative of materials with a porous structure while, for the parent biomass (**Fig. 10**a), they are typical of a non-porous material [71]. The shape of the adsorption branch, which experiences a steep increase of N_2 uptake in the lower relative pressure region ($P{\cdot}P_0^{-1} < 0.05$) and a more gradual increase over the rest of the pressure range, represents a common feature of all the biochar isotherms. This behavior indicates the presence of a large amount of micropores (< 2 nm) and a moderate presence of mesopores (> 2 nm) [71] which is confirmed by the hysteresis loops observed in Fig. 10 over the range $P{\cdot}Po^{-1} =$ 0.4–0.85, especially for BC_3 and BC_4. These loops are typical in nitrogen sorption isotherms that often indicate network effects or various forms of pore blocking due to pore condensation [71]. The desorption branches of BC_3 (Fig. 10d) and BC_4 (Fig. 10e) display a distinct "step" after which they overlap with the adsorption branches. This "step",

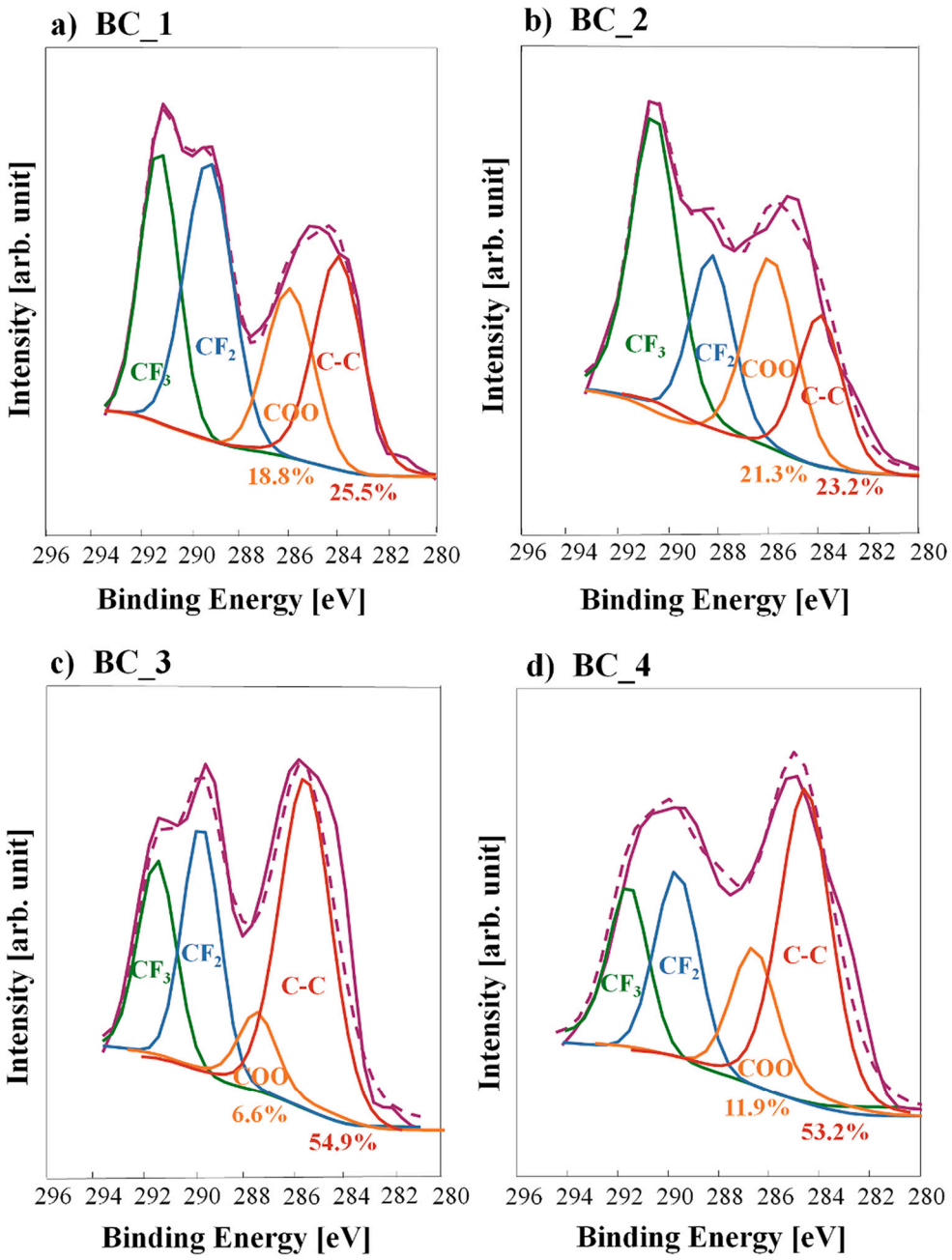

Fig. 8. High resolution C 1 s spectra recorded on the surface of (a) BC_1, (b) BC_2, (c) BC_3 and (d) BC_4. Purple solid line denotes experimental data and dotted its fit after deconvolution of CF_3 (green line), CF_2 (blue line), COO (orange line) and C-C/ C-H (red line). (For interpretation of the references to color in this figure legend, the reader is referred to the web version of this article.)

occurring at a particular relative pressure, confirms the presence of mesopores [71]. The hysteresis loop closely resembles a Type HIV loop [72] which is often found in micro - and mesoporous carbons [71]. The desorption branches of BC_1 and BC_2 also present the characteristic 'step', although they do not overlap with the adsorption branches. This lack of closure can be attributed to diffusion or chemical traps in the biochar as a result of N_2 adsorption which can modify structurally or chemically its surface [73]. The pore blocking that is responsible for these hysteresis loops often originates from ink-bottle-shaped pores, meaning that wide pores can only provide access to the external surface through narrow necks. Similar biochar N_2-physisorpion isotherms behaviours were reported by [18].

The adsorption branches ($0.05 < P{\cdot}P_0^{-1} < 0.2$) presented in Fig. 10 were used to calculate BET specific surface area (SSA) and pore volume (PV). These values are presented in Table 7.

The SSA and the PV values reported in Table 7 confirm the non-porous and porous nature of the biomass and the biochars respectively. Moreover, they are in agreement with our SEM results (Section 3.6 **SEM-EDS**). Air/steam gasification biochars (BC_3 and BC_4) present higher average surface area compared to air gasification ones (BC_1 and BC_2), reaching the highest value (410 $m^2.g^{-1}$), when the highest SB is used (BC_4, SB =1.2). In addition, air/steam gasification biochars present higher PV values compared to literature (Table 1), reaching 197.93 $cm^3.g^{-1}$ for BC_4. The total pore distribution is presented in Fig. 11.

As can be seen in Fig. 11, even though all biochars present a large amount of micropores which are smaller than 1 nm, air/steam gasification biochars (BC_3 and BC_4) exhibit a larger presence of mesopores of about 5 nm compared to air gasification biochars BC_1 and BC_2.

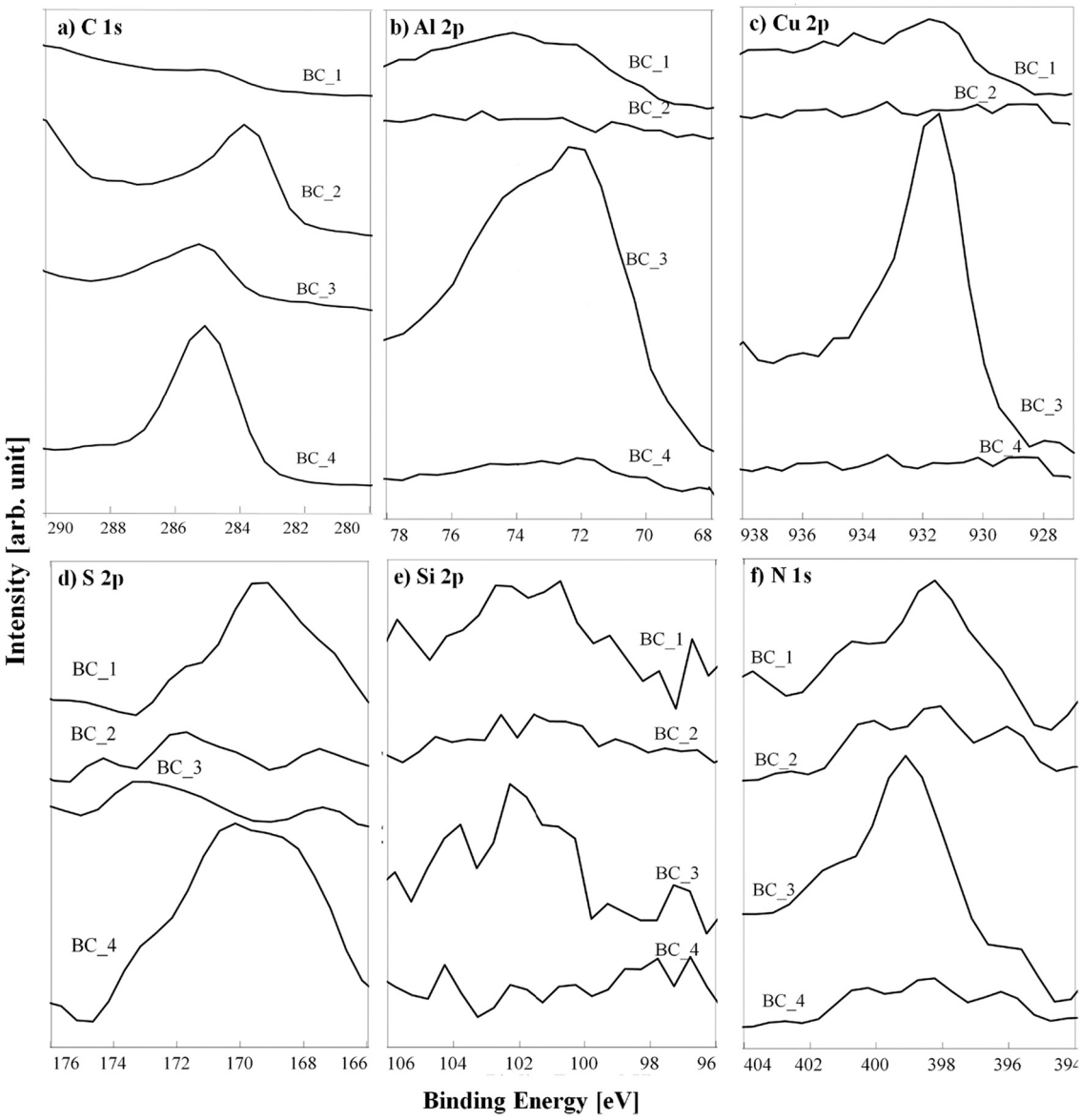

Fig. 9. Non-normalized high-resolution spectra of (a) C 1 s, (b) Al 2p, (c) Cu 2p, (d) S 2p, (e) Si 2p and (f) N 1 s spectra of biochars BC_1, BC_2, BC_3 and BC_4.

Moreover, in this case, the distribution peak decreases when higher λ (BC_2) and SB (BC_4) are considered.

3.9. Potential applications of biochar from the IHBFBSR unit

The IHBFBSR unit produced biochars with carbon content (> 92 wt %), fixed carbon (> 82 wt%) and surface area (> 250 $m^2.g^{-1}$) in the high-end range of the available literature [17,74]. Furthermore, all studied biochars have low ash content (< 9.8 wt%) and thus low content of AAEM species and traces of heavy metals (Ti and Mn) compared to the carbon structure (Table 5 and Fig. 6). This is agreement with biochars from woody biomass reported in literature [17,74]. Based on these data and the robust literature on biochar applications, the IHBFBSR biochars can have potential for: anaerobic digestion (AD) [38], CO_2 capture/removal in wastewater [75], electrochemical applications (carbon fuel cells, electrocatalyst, supercapacitor and carbon nano-tubes [38]), landfill methane mitigation [76,77], soil amendment, solid fuel and tar removal [78], For AD, biochar is used to increase the direct interspecies electron transfer (DIET), providing quicker degradation of substrate and intermediates [79]. Biochars with high degree of aromaticity are known to be beneficial to DIET efficiency [79]. In this sense, air/steam gasification biochars (BC_3 and BC_4) might be suitable for this type of application.

The high C content (Table 4), high proportion of aliphatic C—C (Fig. 8) and larger porous pattern (**Supplementary Fig. G.1**), suggest that BC3 > BC4 could be ideal candidates for CO_2 adsorption [69]. On the other hand, the high content of K_2O (Table 5) in BC_1 > BC_2 compared to BC_3 > BC_4 may exhibit a higher positive effect on CO_2 adsorption, due to increased surface basicity of the biochar [82]. This is also supported by the high proportion of OH^- on the near-surface of BC_2 and BC_3 observed from XPS measurements (Fig. 7), which is known to enhance the alkalinity of the biochar [83].

For electrochemical purposes, the high aromaticity of the studied biochars might prove useful as there is a strong correlation between the degree of aromatization and the dielectric constant of biochar [84]. Thus, based on the O/C and HC ratios our biochars are ranked from the highest to the lowest degree of aromaticity: BC_4 > BC3 > BC_2 > BC_1.

Biochars with large surface area are also known to be good sorbent materials for heavy metals and organic contamination [85], such as BC_3 > BC_4. Further, when biochar has particle sizes lower than 1 mm,

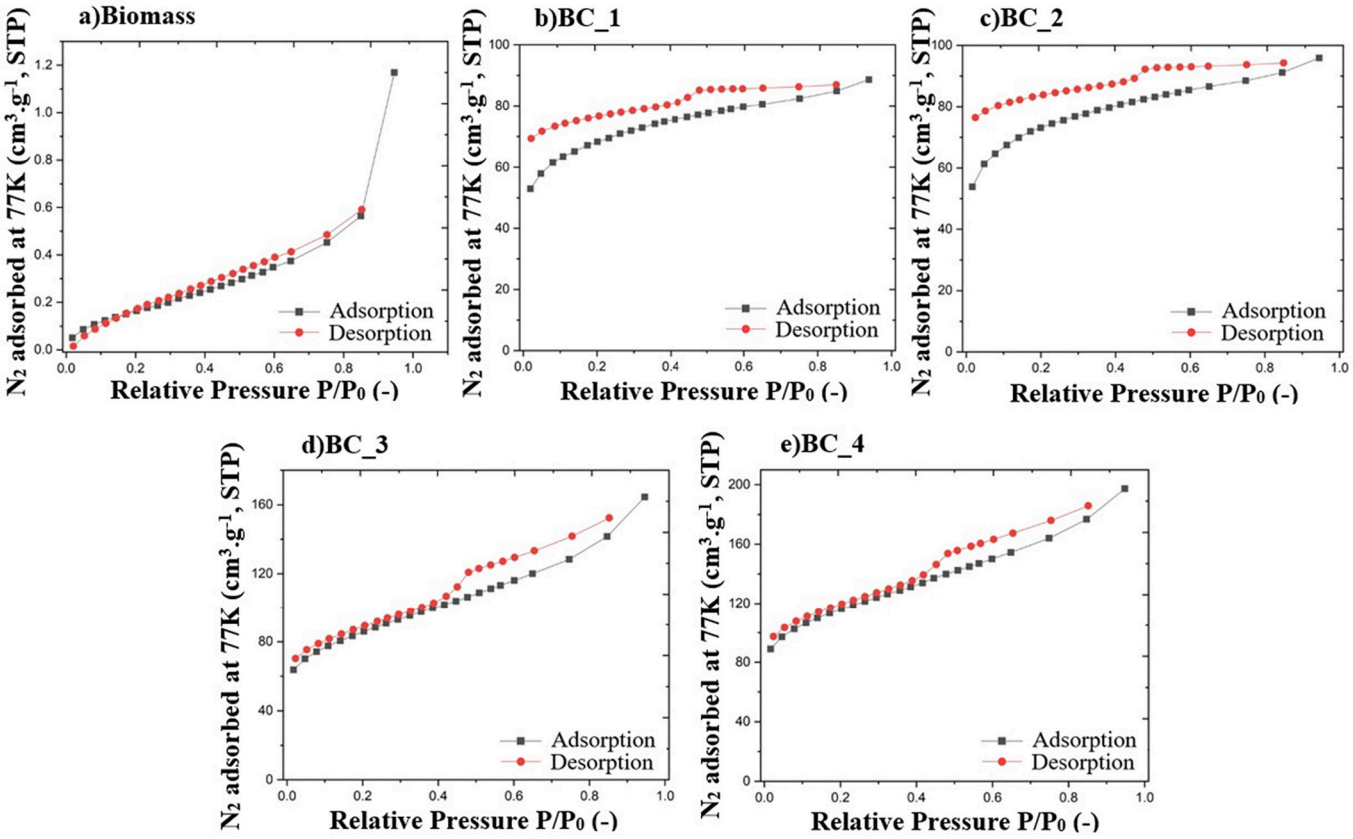

Fig. 10. N_2-physisorpion isotherms measured at 77 K of biomass and biochars BC_1–4.

Table 7
SSA and PV of biomass and biochars BC_1–4.

	Biomass	BC_1	BC_2	BC_3	BC_4
Specific surface area ($m^2.g^{-1}$)					
SSA	0.17	250	260	300	410
Pore volume ($cm^3.g^{-1}$)					
PV[a]	1.12	88.66	95.87	164.45	197.93

[a] Values obtained from the amount of N_2 adsorbed at $P{\cdot}P_0^{-1} = 0.95$.

it has an equal performance of filtration efficiency with that of activated carbon [86]. Thus, our biochars are ranked from the highest to the lowest according to the wt% content of sieved particles reported in Fig. 4-: BC_3 > BC_4 > BC_1 > BC_2. The biochars produced in this work with sieve particle sizes between 500 and 850 μm and pore volume in the range of 88–197 $cm^3.g^{-1}$ could, therefore, be of use in filtration applications.

As solid fuel candidates, the studied biochars are ranked according to their O/C ratio and HHV: BC_4 > BC3 > BC_2 > BC_1. Major obstacles related to the inorganic content of the biochars are discarded since their ash content is relatively low, especially for BC_3 and BC_4 (<5 wt% a.r.). Further, the presence of CaO (Table 5) in all studied biochars might

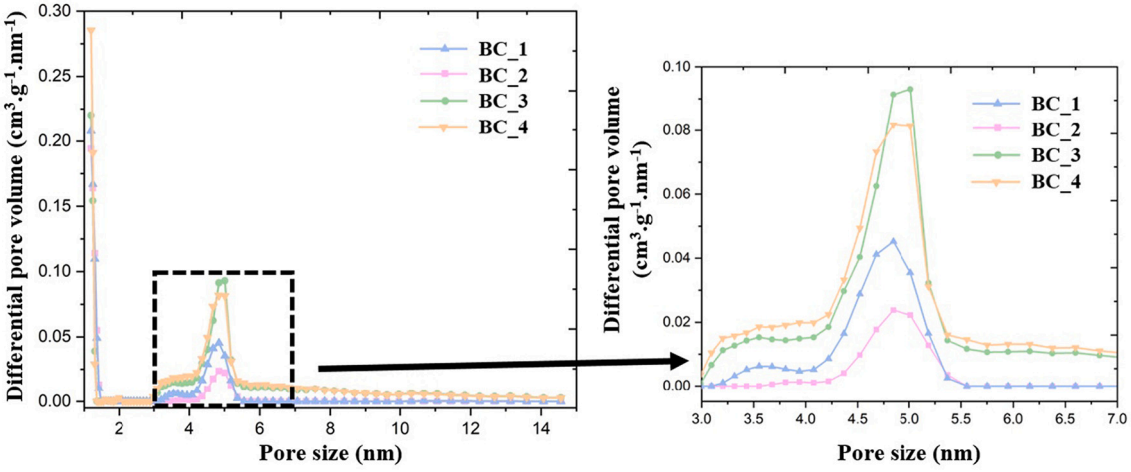

Fig. 11. Pore size distribution (PSD) of biochars BC_1–4, obtained from the N_2-physisorpion isotherms.

prevent agglomeration and fouling when used as solid fuel [80]. With respect to K_2O (Table 5), this is found in the biochars below the threshold for slagging problems [81].

Biochars with a high degree of aromaticity and high fixed carbon content are known to have increased resistance to chemical oxidation and microbial mineralization [17,38]. The high C content of the studied biochars also suggests that the labile fraction of the biochars could be relatively small preventing offset of the carbon sequestration benefits and preventing short-term degradability [87]. Nevertheless, it is important that biochar is still capable of hosting microorganisms and water to preserve the flora of the soil and promote plant growth [88]. Thus, based on SEM images (**Supplementary Fig. G.1**) and BET analysis (Table 7), BC_3 and BC_4 might provide better "habitability" compared to BC_1 and BC_2. Furthermore, the high proportion of semicrystalline C (cellulose and crystalline carbon) found in XRD patterns (Fig. 5) also supports the hypothesis that the investigated biochars will be more resistant to degradation in soil, especially BC_3 > BC_2 [89]. Yet, further research is needed to evaluate if the high crystallinity of the biochars could reduce properties such as water holding capacity or nutrient retention once added to the soil. The Ca and K found as minor components (Table 5 and Fig. 6) in the biochars might also prove beneficial as nutrients for plant growth. Nevertheless, further research is needed regarding the effects of these elements in soil as well as role of the heavy metals detected trace concentrations (Ti and Mn). The presence of heavy metals in biochar is a challenge but a recent study [85] indicates that highly aromatic biochars, as the ones produced in our work, can form a more stable bond of heavy metal complexing agent reducing the risk of heavy metal mobilization. The high proportion of O-containing functional groups in BC_2 > BC_1 suggests a higher cation exchange capacity [10] compared to BC_3 and BC_4 which could lead to increased nutrient holding and reduced leaching [90]. Yet, these functional groups might lower the stability of BC_2 > BC_1 against degradation in soil [91]. Thus, for soil amendment applications, the studied biochars were ranked as follow: BC_3 > BC_4 > BC_1 > BC_2.

4. Conclusions and outlook

This work focused on valorizing wood-derived biochars obtained with a novel 50 kW_{th} pilot plant IHBFBSR via gasification. We investigated four different biochars produced at different production conditions and proposed post process applications depending on physicochemical properties. Our findings confirm that the IHBFBSR design constitutes a promising development for the production of biochar with higher carbon content (> 92%) and high porosity (89–198 $cm^3.g^{-1}$) compared to other designs in literature.

In particular, our results indicate that:

1) Steam gasification is recommended when a larger porous structure and high fixed carbon content are required. The IHBFBSR also produces a porous biochar with no sign of pore clogging.
2) The properties of air/steam biochars produced by the IHBFBSR are promising for larger portfolio of applications compared to the air ones such as: CO_2 capture, electrochemical applications, soil amendment, sorbent material for heavy metals, landfill methane mitigation, tar removal, anaerobic digestion and filtration media.

High quality biochars can contribute on improving the circularity of the gasification and mitigating climate change.

Nomenclature

a.r.	As Received Basis
AAEM	Alkali and Alkali Earth Metals
AD	Anaerobic Digestion
d.a.f.	Dry Ash Free Basis
d.b.	Dry Basis
DIET	Direct Interspecies Electron Transfer
BC_i $i = 1, \ldots,4$	Biochar Materials Analyzed
Bed_i i = A, B	Bed Material Used
BET	Brunauer-Emmet-Teller
CYC0i i = 1, …,2	Cyclones
EH0i i = 1, …,2	Preheater
GC	Gas Chromatograph
GHG	Greenhouse Gases
IHBFBSR	Indirectly Heated Bubbling Fluidized Bed Steam Reformer
FTIR	Fourier Transform Infrared
NDIR	Nondispersive Infrared Sensor
NMR	Nuclear Magnetic Resonance Spectroscopy
PMMA	Poly(methyl methacrylate)
PSD	Particle size Distribution
QSDFT	Quenched Solid Density Functional Theory
ROI	Regions of Interests
SB0i i = 1, …,5	Feeding System Bunker
SEM-EDS	Scanning Electron Microscopy and Energy Dispersive X-ray Spectroscopy
TU Delft	Deft University of Technology
XPS	X-ray Photoelectron Spectroscopy
XRF	X-ray Fluorescence

Parameters (Units)

CC	Carbon Conversion Efficiency (%)
CGE	Cold Gas Efficiency (%)
H/C	Hydrogen/Carbon Molar Ratio (–)
HHV	High Heating Value ($MJ.kg^{-1}$)
O/C	Oxygen/Carbon Molar Ratio (–)
N/C	Nitrogen/Carbon Molar Ratio (–)
P	Process Pressure (atm)
P/P_0	Relative Pressure (–)
PSD	Pore Size Distribution (nm)
PV	Pore Volume ($cm^3.g^{-1}$)
SB	Steam to Biomass Ratio (–)
SSA	Specific Surface Area ($m^2.g^{-1}$)
T	Process Temperature ($^{\circ}C$)
$Y_{BC,i\ lost}$ $i = 1, \ldots,4$	Mass Yield of Biochar Lost (%)
$Y_{BC,i\ net}$ $i = 1, \ldots,4$	Mass Yield of Biochar for Further Applications (%)
$Y_{BC,i\ tot}$ $i = 1, \ldots,4$	Total Mass Yield of Biochar (%)

Greek symbols (Units)

λ	Equivalent Ratio (–)

Funding

This work was co-financed by the Dutch company Petrogas – Gas Systems.

CRediT authorship contribution statement

Mara Del Grosso: Conceptualization, Methodology, Investigation, Validation, Writing – original draft, Visualization. **Luis Cutz:** Conceptualization, Methodology, Investigation, Validation, Writing – original draft, Visualization. **Urša Tiringer:** Conceptualization, Methodology, Investigation, Validation, Writing – original draft, Visualization. **Christos Tsekos:** Investigation, Writing – review & editing. **Peyman Taheri:** Writing – review & editing, Supervision. **Wiebren de Jong:** Writing – review & editing, Supervision, Project administration, Funding acquisition.

Declaration of Competing Interest

The authors declare that they have no known competing financial

interests or personal relationships that could have appeared to influence the work reported in this paper.

Acknowledgments

The authors would like to thank Mr. Ruud Hendrikx (Department of Material Science and Engineering – TU Delft) for performing the XRD and XRD tests and PhD Candidate Hugo Veldhuizen (Faculty of Aerospace Engineering – TU Delft) for performing the N_2-physisorption tests.

Appendix A. Supplementary data

Supplementary data to this article can be found online at https://doi.org/10.1016/j.fuproc.2022.107347.

References

[1] M. Guo, W. Song, J. Buhain, Bioenergy and biofuels: history, status, and perspective, Renew. Sust. Energ. Rev. 42 (2015) 712–725, https://doi.org/10.1016/j.rser.2014.10.013.
[2] Q. Liu, S.C. Chmely, N. Abdoulmoumine, Biomass treatment strategies for thermochemical conversion, Energy Fuel 31 (2017) 3525–3536, https://doi.org/10.1021/acs.energyfuels.7b00258.
[3] W. de Jong, J.R. van Ommen, Biomass as a Sustainable Energy Source for the Future: Fundamentals of Conversion Processes, John Wiley & Sons, 2014.
[4] H.S. Kambo, A. Dutta, A comparative review of biochar and hydrochar in terms of production, physico-chemical properties and applications, Renew. Sust. Energ. Rev. 45 (2015) 359–378, https://doi.org/10.1016/j.rser.2015.01.050.
[5] W.-J. Liu, H. Jiang, H.-Q. Yu, Development of biochar-based functional materials: toward a sustainable platform carbon material, Chem. Rev. 115 (2015) 12251–12285, https://doi.org/10.1021/acs.chemrev.5b00195.
[6] J. Lee, A.K. Sarmah, E.E. Kwon, Production and Formation of Biochar, in: Biochar from Biomass and Waste, Elsevier, 2019, pp. 3–18, https://doi.org/10.1016/B978-0-12-811729-3.00001-7.
[7] H. Boerrigter, R. Rauch, Review of applications of gases from biomass gasification, 2006, p. 33.
[8] P.J. Woolcock, R.C. Brown, A review of cleaning technologies for biomass-derived syngas, Biomass Bioenergy 52 (2013) 54–84, https://doi.org/10.1016/j.biombioe.2013.02.036.
[9] P. Definition, S. Standards, Standardized Product Definition and Product Testing Guidelines for Biochar That Is Used in Soil, 2015, pp. 1–61.
[10] J.W. Lee, M. Kidder, B.R. Evans, S. Paik, A.C. Buchanan III, C.T. Garten, R. C. Brown, Characterization of Biochars Produced from Cornstovers for Soil Amendment, Environ. Sci. Technol. 44 (2010) 7970–7974, https://doi.org/10.1021/es101337x.
[11] H. Schmidt, 55 Uses of Biochar, Ithaka J. (2012) 286–289.
[12] V. Hansen, D. Müller-Stöver, J. Ahrenfeldt, J.K. Holm, U.B. Henriksen, H. Hauggaard-Nielsen, Gasification biochar as a valuable by-product for carbon sequestration and soil amendment, Biomass Bioenergy 72 (2015) 300–308, https://doi.org/10.1016/j.biombioe.2014.10.013.
[13] D. Woolf, J.E. Amonette, F.A. Street-Perrott, J. Lehmann, S. Joseph, Sustainable biochar to mitigate global climate change, Nat. Commun. 1 (2010) 56, https://doi.org/10.1038/ncomms1053.
[14] V. Benedetti, E. Cordioli, F. Patuzzi, M. Baratieri, CO_2 Adsorption study on pure and chemically activated chars derived from commercial biomass gasifiers, J. CO2 Utiliz. 33 (2019) 46–54, https://doi.org/10.1016/j.jcou.2019.05.008.
[15] C.E. Brewer, K. Schmidt-Rohr, J.A. Satrio, R.C. Brown, Characterization of biochar from fast pyrolysis and gasification systems, Environ. Prog. Sustain. Energy 28 (2009) 386–396, https://doi.org/10.1002/ep.10378.
[16] D.P. Cole, E.A. Smith, Y.J. Lee, High-resolution mass spectrometric characterization of molecules on biochar from pyrolysis and gasification of switchgrass, Energy Fuel 26 (2012) 3803–3809, https://doi.org/10.1021/ef300356u.
[17] L. Fryda, R. Visser, Biochar for Soil Improvement: Evaluation of Biochar from Gasification and Slow Pyrolysis, Agriculture. 5 (2015) 1076–1115, https://doi.org/10.3390/agriculture5041076.
[18] X. Meng, Biomass gasification: the understanding of sulfur, tar, and char reaction in fluidized bed gasifiers, 2012, p. 271.
[19] R. Muvhiiwa, A. Kuvarega, E.M. Llana, A. Muleja, Study of biochar from pyrolysis and gasification of wood pellets in a nitrogen plasma reactor for design of biomass processes, J. Environ. Chem. Eng. 7 (2019), 103391, https://doi.org/10.1016/j.jece.2019.103391.
[20] C.E. Brewer, K. Schmidt-Rohr, J.A. Satrio, R.C. Brown, Characterization of biochar from fast pyrolysis and gasification systems, Environ. Prog. Sustain. Energy 28 (2009) 386–396, https://doi.org/10.1002/ep.10378.
[21] C. Tsekos, M. del Grosso, W. de Jong, Gasification of woody biomass in a novel indirectly heated bubbling fluidized bed steam reformer, Fuel Process. Technol. 224 (2021), 107003, https://doi.org/10.1016/j.fuproc.2021.107003.
[22] M. Farris, M.A. Paisley, J. Irving, R.P. Overend, The Biomass Gasification Process by Battelle/Ferco: Design, Engineering, Construction and Startup, 1998, p. 13.
[23] H. Hofbauer, G. Veronik, T. Fleck, R. Rauch, H. Mackinger, E. Fercher, The FICFB — gasification process, in: A.V. Bridgwater, D.G.B. Boocock (Eds.), Developments in Thermochemical Biomass Conversion, Springer Netherlands, Dordrecht, 1997, pp. 1016–1025, https://doi.org/10.1007/978-94-009-1559-6_82.
[24] C.M. van der Meijden, Development of the MILENA gasification technology for the production of Bio-SNG, Technische Universiteit Eindhoven, 2010.
[25] FEPA, Corundum Datasheet, Federation of European Producers of Abrasives. www.unicorn-ics.nl, 2017 (accessed November 7, 2017).
[26] Sluiter, et al., Determination of Ash in Biomass: Laboratory Analytical Procedure (LAP); Issue Date: 7/17/2005, Technical Report 8, 2008.
[27] Sluiter, et al., Determination of Total Solids in Biomass and Total Dissolved Solids in Liquid Process Samples: Laboratory Analytical Procedure (LAP), Technical Report, 2008, p. 9.
[28] J.I. Goldstein, D.E. Newbury, J.R. Michael, N.W.M. Ritchie, J.H.J. Scott, D.C. Joy, Scanning Electron Microscopy and X-Ray Microanalysis, Springer, 2017.
[29] S.K. Buratto, Engineering the next generation, Nat. Nanotechnol. 5 (2010) 176, https://doi.org/10.1038/nnano.2010.39.
[30] J. Wielant, T. Hauffman, O. Blajiev, R. Hausbrand, H. Terryn, Influence of the Iron Oxide Acid−Base Properties on the Chemisorption of Model Epoxy Compounds Studied by XPS, J. Phys. Chem. C 111 (2007) 13177–13184, https://doi.org/10.1021/jp072354j.
[31] E. Lugato, F.P. Vaccari, L. Genesio, S. Baronti, A. Pozzi, M. Rack, J. Woods, G. Simonetti, L. Montanarella, F. Miglietta, An energy-biochar chain involving biomass gasification and rice cultivation in Northern Italy, GCB Bioenergy 5 (2013) 192–201, https://doi.org/10.1111/gcbb.12028.
[32] J.R. Jenkins, M. Viger, E.C. Arnold, Z.M. Harris, M. Ventura, F. Miglietta, C. Girardin, R.J. Edwards, C. Rumpel, F. Fornasier, C. Zavalloni, G. Tonon, G. Alberti, G. Taylor, Biochar alters the soil microbiome and soil function: results of next-generation amplicon sequencing across Europe, GCB Bioenergy 9 (2017) 591–612, https://doi.org/10.1111/gcbb.12371.
[33] M. Siedlecki, On the gasification of biomass in a steam-oxygen blown CFB gasifier with the focus on gas quality upgrading: technology background, experiments and mathematical modeling., [s.n.], 2011.
[34] K. Weber, P. Quicker, Properties of biochar, Fuel. 217 (2018) 240–261, https://doi.org/10.1016/j.fuel.2017.12.054.
[35] P. Basu, Gasification Theory, in: Biomass Gasification, Pyrolysis and Torrefaction, Elsevier, 2013, pp. 199–248, https://doi.org/10.1016/B978-0-12-396488-5.00007-1.
[36] A. Kumar, K. Eskridge, D.D. Jones, M.A. Hanna, Steam–air fluidized bed gasification of distillers grains: Effects of steam to biomass ratio, equivalence ratio and gasification temperature, Bioresour. Technol. 100 (2009) 2062–2068, https://doi.org/10.1016/j.biortech.2008.10.011.
[37] EBC, European Biochar Certificate - Guidelines for a Sustainable Production of Biochar, European Biochar Certificate (EBC), Arbaz, Switzerland, 2012.
[38] S. You, Y.S. Ok, S.S. Chen, D.C.W. Tsang, E.E. Kwon, J. Lee, C.-H. Wang, A critical review on sustainable biochar system through gasification: Energy and environmental applications, Bioresour. Technol. 246 (2017) 242–253, https://doi.org/10.1016/j.biortech.2017.06.177.
[39] M. Prins, K. Ptasinski, F. Janssen, From coal to biomass gasification: Comparison of thermodynamic efficiency, Energy. 32 (2007) 1248–1259, https://doi.org/10.1016/j.energy.2006.07.017.
[40] K.A. Spokas, Review of the stability of biochar in soils: predictability of O:C molar ratios, Carbon Managem. 1 (2010) 289–303, https://doi.org/10.4155/cmt.10.32.
[41] N.A. Qambrani, Md.M. Rahman, S. Won, S. Shim, C. Ra, Biochar properties and eco-friendly applications for climate change mitigation, waste management, and wastewater treatment: a review, Renew. Sust. Energ. Rev. 79 (2017) 255–273, https://doi.org/10.1016/j.rser.2017.05.057.
[42] O. Mašek, W. Buss, P. Brownsort, M. Rovere, A. Tagliaferro, L. Zhao, X. Cao, G. Xu, Potassium doping increases biochar carbon sequestration potential by 45%, facilitating decoupling of carbon sequestration from soil improvement, Sci. Rep. 9 (2019) 5514, https://doi.org/10.1038/s41598-019-41953-0.
[43] K. Wiedner, C. Rumpel, C. Steiner, A. Pozzi, R. Maas, B. Glaser, Chemical evaluation of chars produced by thermochemical conversion (gasification, pyrolysis and hydrothermal carbonization) of agro-industrial biomass on a commercial scale, Biomass Bioenergy 59 (2013) 264–278, https://doi.org/10.1016/j.biombioe.2013.08.026.
[44] IPCC, Chapter 8, in: Climate Change 2013: The Physical Science Basis. Contribution of Working Group I to the Fifth Assessment Report of the Intergovernmental Panel on Climate Change, Cambridge University Press, 2013.
[45] E.M.C.C. Batista, J. Shultz, T.T.S. Matos, M.R. Fornari, T.M. Ferreira, B. Szpoganicz, R.A. de Freitas, A.S. Mangrich, Effect of surface and porosity of biochar on water holding capacity aiming indirectly at preservation of the Amazon biome, Sci. Rep. 8 (2018), https://doi.org/10.1038/s41598-018-28794-z.
[46] F.J. Stevenson, M.A. Cole, Cycles of Soils: Carbon, Nitrogen, Phosphorus, Sulfur, Micronutrients, 2nd edition, Wiley, 1999. https://www.wiley.com/en-us/Cycles+of+Soils%3A+Carbon%2C+Nitrogen%2C+Phosphorus%2C+Sulfur%2C+Micronutrients%2C+2nd+Edition-p-9780471320715 (accessed March 24, 2021).
[47] T. Deluca, M.J. Gundale, M.D. Mackenzie, D. Jones, Biochar effects on soil nutrient transformations, in, 2015, pp. 421–454.
[48] C. Steiner, W.G. Teixeira, J. Lehmann, T. Nehls, J.L.V. de Macêdo, W.E.H. Blum, W. Zech, Long term effects of manure, charcoal and mineral fertilization on crop production and fertility on a highly weathered Central Amazonian upland soil, Plant Soil 291 (2007) 275–290, https://doi.org/10.1007/s11104-007-9193-9.
[49] K.Y. Chan, Z. Xu, Biochar: Nutrient Properties and their Enhancement, in: Biochar for Environmental Management, Routledge, 2009.

[50] M.L. Cayuela, M.A. Sánchez-Monedero, A. Roig, K. Hanley, A. Enders, J. Lehmann, Biochar and denitrification in soils: when, how much and why does biochar reduce N2O emissions? Sci. Rep. 3 (2013) 1732, https://doi.org/10.1038/srep01732.
[51] J.W. Gaskin, C. Steiner, K. Harris, K.C. Das, B. Bibens, Effect of low-temperature pyrolysis conditions on biochar for agricultural use, Trans. ASABE 51 (2008) 2061–2069, https://doi.org/10.13031/2013.25409.
[52] M. Bläsing, M. Zini, M. Müller, Influence of feedstock on the release of potassium, sodium, chlorine, sulfur, and phosphorus species during gasification of wood and biomass shells, Energy Fuel 27 (2013) 1439–1445, https://doi.org/10.1021/ef302093r.
[53] Y. Wang, L. Qiu, M. Zhu, G. Sun, T. Zhang, K. Kang, Comparative evaluation of hydrothermal carbonization and low temperature pyrolysis of *Eucommia ulmoides* Oliver for the production of solid biofuel, Sci. Rep. 9 (2019) 5535, https://doi.org/10.1038/s41598-019-38849-4.
[54] J.S. Clemente, S. Beauchemin, Y. Thibault, T. MacKinnon, D. Smith, Differentiating Inorganics in Biochars Produced at Commercial Scale using principal Component Analysis, ACS Omega. 3 (2018) 6931–6944, https://doi.org/10.1021/acsomega.8b00523.
[55] B. Zhao, O.D. Nartey, Characterization and Evaluation of Biochars Derived from Agricultural Waste Biomass from Gansu, China, 2014, p. 17.
[56] T.R. Pacioni, D. Soares, M.D. Domenico, M.F. Rosa, R.F.P.M. De Moreira, H.J. José, Bio-syngas production from agro-industrial biomass residues by steam gasification, Waste Manag. 58 (2016) 221–229, https://doi.org/10.1016/j.wasman.2016.08.021.
[57] F. Heras, N. Alonso, M.Á. Gilarranz, J.J. Rodriguez, Activation of waste tire char upon cyclic oxygen chemisorption−desorption, Ind. Eng. Chem. Res. 48 (2009) 4664–4670, https://doi.org/10.1021/ie801764x.
[58] A.F. Ismail, K. Khulbe, T. Matsuura, Gas Separation Membranes: Polymeric and Inorganic, Springer International Publishing, 2015, https://doi.org/10.1007/978-3-319-01095-3.
[59] C. Di Blasi, Combustion and gasification rates of lignocellulosic chars, Prog. Energy Combust. Sci. 35 (2009) 121–140, https://doi.org/10.1016/j.pecs.2008.08.001.
[60] X. Qi, G. Song, W. Song, S. Yang, Effect of bed materials on slagging and fouling during Zhundong coal gasification, Energy Explor. Exploit. 35 (2017) 558–578.
[61] R. Michel, J. Kaknics, E. de Bilbao, J. Poirier, The mechanism of agglomeration of the refractory materials in a fluidized-bed reactor, Ceram. Int. 42 (2016) 2570–2581, https://doi.org/10.1016/j.ceramint.2015.10.060.
[62] G. Song, X. Qi, W. Song, Q. Lu, Slagging characteristics of zhundong coal during circulating fluidized bed gasification, Energy Fuel 30 (2016) 3967–3974, https://doi.org/10.1021/acs.energyfuels.6b00503.
[63] E. McCafferty, J.P. Wightman, Determination of the concentration of surface hydroxyl groups on metal oxide films by a quantitative XPS method, Surface and Interface, Analysis. 26 (1998) 549–564, https://doi.org/10.1002/(SICI)1096-9918(199807)26:8<549::AID-SIA396>3.0.CO;2-Q.
[64] N.A. Zubbri, A.R. Mohamed, N. Kamiuchi, M. Mohammadi, Enhancement of CO2 adsorption on biochar sorbent modified by metal incorporation, Environ. Sci. Pollut. Res. 27 (2020) 11809–11829, https://doi.org/10.1007/s11356-020-07734-3.
[65] R.V. Lakshmi, S.T. Aruna, C. Anandan, P. Bera, S. Sampath, EIS and XPS studies on the self-healing properties of Ce-modified silica-alumina hybrid coatings: evidence for Ce(III) migration, Surf. Coat. Technol. 309 (2017) 363–370, https://doi.org/10.1016/j.surfcoat.2016.11.051.
[67] Spectral Interpretation, In: X-Ray Photoelectron Spectroscopy, John Wiley & Sons, Ltd, 2011, pp. 101–140, https://doi.org/10.1002/9781118162897.ch5.
[68] NIST, X-Ray Photoelectron Spectroscopy (XPS) Database Main Search Menu. https://srdata.nist.gov/xps/main_search_menu.aspx, 2021.
[69] A.D. Igalavithana, S.W. Choi, P.D. Dissanayake, J. Shang, C.-H. Wang, X. Yang, S. Kim, D.C.W. Tsang, K.B. Lee, Y.S. Ok, Gasification biochar from biowaste (food waste and wood waste) for effective CO2 adsorption, J. Hazard. Mater. 391 (2020), 121147, https://doi.org/10.1016/j.jhazmat.2019.121147.
[70] J. Guo, B. Chen, Insights on the Molecular Mechanism for the Recalcitrance of Biochars: Interactive Effects of Carbon and Silicon Components, Environ. Sci. Technol. 48 (2014) 9103–9112, https://doi.org/10.1021/es405647e.
[71] M. Thommes, K. Kaneko, A.V. Neimark, J.P. Olivier, F. Rodriguez-Reinoso, J. Rouquerol, K.S.W. Sing, Physisorption of gases, with special reference to the evaluation of surface area and pore size distribution (IUPAC Technical Report), Pure and Applied, Chemistry. 87 (2015) 1051–1069, https://doi.org/10.1515/pac-2014-1117.
[72] J. Lykiema, K.S.W. Sing, J. Haber, M. Kerker, E. Wolfram, J.H. Block, N. V. Churaev, D.H. Everett, R.S. Hansen, R.A.W. Haul, J.W. Hightower, R.J. Hunter, Prepared for publication by the Subcommittee on Reporting Gas Adsorption Data Consisting of K. S. W. SING (UK, Chairman); D. H. EVERETT (UK); R. A. W. HAUL (FRG); L. MOSCOU (Netherlands); R. A. PIEROTTI (USA); J. ROUQUEROL (France); T. SIEMIENIEWSKA (Poland), 1984, p. 17.
[73] V.V. Kutarov, E. Robens, Yu.I. Tarasevich, E.V. Aksenenko, Adsorption hysteresis at low relative pressures, Theor. Exp. Chem. 47 (2011) 163, https://doi.org/10.1007/s11237-011-9198-6.
[74] B. Song, X. Cao, W. Gao, S. Aziz, S. Gao, C.-H. Lam, R. Lin, Preparation of nano-biochar from conventional biorefineries for high-value applications, Renew. Sust. Energ. Rev. 157 (2022), 112057, https://doi.org/10.1016/j.rser.2021.112057.
[75] Y. Shen, J.L. Linville, P.A.A. Ignacio-de Leon, R.P. Schoene, M. Urgun-Demirtas, Towards a sustainable paradigm of waste-to-energy process: Enhanced anaerobic digestion of sludge with woody biochar, J. Clean. Prod. 135 (2016) 1054–1064, https://doi.org/10.1016/j.jclepro.2016.06.144.
[76] M. Huber-Humer, J. Gebert, H. Hilger, Biotic systems to mitigate landfill methane emissions, Waste Manag. Res. 26 (2008) 33–46, https://doi.org/10.1177/0734242X07087977.
[77] Q. Zhao, Y. Wang, Z. Xu, Z. Yu, How does biochar amendment affect soil methane oxidation? A review, J. Soils Sediments 21 (2021) 1575–1586, https://doi.org/10.1007/s11368-021-02889-z.
[78] Z. El-Rub, E. Bramer, G. Brem, Experimental comparison of biomass chars with other catalysts for tar reduction, Fuel. 87 (2008) 2243–2252.
[79] Q. Qi, C. Sun, C. Cristhian, T. Zhang, J. Zhang, H. Tian, Y. He, Y.W. Tong, Enhancement of methanogenic performance by gasification biochar on anaerobic digestion, Bioresour. Technol. 330 (2021), 124993, https://doi.org/10.1016/j.biortech.2021.124993.
[80] J.D. Martínez-Ángel, R.A. Villamizar-Gallardo, O.O. Ortíz-Rodríguez, Characterization and evaluation of cocoa (*Theobroma cacao* L.) pod husk as a renewable energy source, Agrociencia. 49 (2015) 329–345.
[81] I. Obernberger, T. Brunner, G. Bärnthaler, Chemical properties of solid biofuels—significance and impact, Biomass Bioenergy 30 (2006) 973–982, https://doi.org/10.1016/j.biombioe.2006.06.011.
[82] G. Yin, Z. Liu, Q. Liu, W. Wu, The role of different properties of activated carbon in CO2 adsorption, Chem. Eng. J. 230 (2013) 133–140, https://doi.org/10.1016/j.cej.2013.06.085.
[83] D.B. Wiedemeier, S. Abiven, W.C. Hockaday, M. Keiluweit, M. Kleber, C. A. Masiello, A.V. McBeath, P.S. Nico, L.A. Pyle, M.P.W. Schneider, R.J. Smernik, G. L.B. Wiesenberg, M.W.I. Schmidt, Aromaticity and degree of aromatic condensation of char, Org. Geochem. 78 (2015) 135–143, https://doi.org/10.1016/j.orggeochem.2014.10.002.
[84] H. Wang, L. Zhang, C. Hu, X. Wang, L. Lyu, G. Sheng, Enhanced degradation of organic pollutants over Cu-doped LaAlO3 perovskite through heterogeneous Fenton-like reactions, Chem. Eng. J. 332 (2018) 572–581, https://doi.org/10.1016/j.cej.2017.09.058.
[85] Y. Zong, Q. Xiao, S. Lu, Biochar derived from cadmium-contaminated rice straw at various pyrolysis temperatures: Cadmium immobilization mechanisms and environmental implication, Bioresour. Technol. 321 (2021), 124459, https://doi.org/10.1016/j.biortech.2020.124459.
[86] C. Berger, Biochar and activated carbon filters for greywater treatment, 2012:14 (2012). https://stud.epsilon.slu.se/5183/ (accessed April 28, 2021).
[87] E.W. Bruun, H. Hauggaard-Nielsen, N. Ibrahim, H. Egsgaard, P. Ambus, P. A. Jensen, K. Dam-Johansen, Influence of fast pyrolysis temperature on biochar labile fraction and short-term carbon loss in a loamy soil, Biomass Bioenergy 35 (2011) 1182–1189, https://doi.org/10.1016/j.biombioe.2010.12.008.
[88] J. Thies, M. Rillig, in: Johannes Lehmann, Stephen Joseph (Eds.), Characteristics of Biochar: Biological Properties, in: Biochar for Environmental Management, Earthscan, London, 2009.
[89] W. Mahmood, M.A. Ariffin, Z. Harun, N. Ishak, J.A. Ghani, M.N.A. Rahman, Characterisation and potential use of biochar from gasified oil palm wastes, J. Eng. Sci. Technol. (2015) 45–54.
[90] J. Major, C. Steiner, A. Downie, J. Lehmann, Biochar Effects on Nutrient Leaching, Routledge, 2009, https://doi.org/10.4324/9781849770552-22.
[91] A.B. Fuertes, M.C. Arbestain, M. Sevilla, J.A. Maciá-Agulló, S. Fiol, R. López, R. J. Smernik, W.P. Aitkenhead, F. Arce, F. Macias, A.B. Fuertes, M.C. Arbestain, M. Sevilla, J.A. Maciá-Agulló, S. Fiol, R. López, R.J. Smernik, W.P. Aitkenhead, F. Arce, F. Macias, Chemical and structural properties of carbonaceous products obtained by pyrolysis and hydrothermal carbonisation of corn Stover, Soil Res. 48 (2010) 618–626, https://doi.org/10.1071/SR10010.